

Chapter Two: Imidazolium Structure Directing Agents in Molecular Sieve Synthesis: Exploring Guest/Host Relationships in the Synthesis of SSZ-70

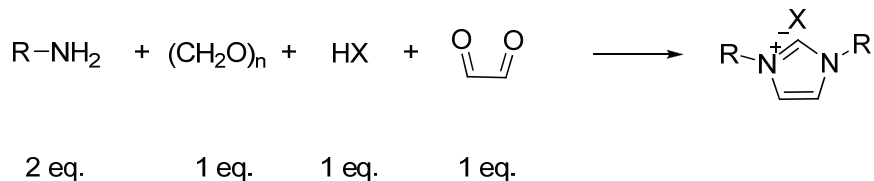
This chapter is reproduced in part with permission from Chemistry of Materials, submitted for publication. Unpublished work copyright 2009 American Chemical Society.

2.1: Introduction

The synthesis of novel molecular sieves has relied on combining an organic structure directing agent (SDA) with appropriate inorganic reaction conditions. The combination of high boron to silica ratios and fluoride lead to a new material denoted SSZ-70¹. The synthesis employed 1,3-diisopropylimidazolium hydroxide as SDA with previous studies showing strong specificity to ZSM-23 (MTT)¹ materials^{2,3}. The MTT framework comprises an undulating one-dimensional pore topology delimited by 10 tetrahedral atoms (10MR) with 5Å periodicity. Single crystal X-ray diffraction studies show the spacing between isopropyl groups is well aligned with the framework periodicity. Furthermore, this observation was used to predict suitable SDAs for MTT synthesis⁴. Given the strong structure directing ability to MTT we were interested if SSZ-70 showed similar framework periodicity.

¹ Molecular sieve frameworks are denoted by three-letter codes assigned by the Structure Commission of the International Zeolite Association. The full structure database can be found at <http://www.iza-structure.org/databases/>.

In addition to the structure directing ability of 1,3-diisopropylimidazolium, several other imidazolium SDAs give the same product across all dilutions under pure silica fluoride synthesis conditions⁵. The majority of organic SDAs studied do not give the same product across all water-to-silica ratios, with low framework density products favored at low H₂O/SiO₂ ratios (<4) and relatively high framework density products at high H₂O/SiO₂ (>14). The imidazolium SDAs discussed above were synthesized via imidazole or substituted imidazole quaternization with an alkyl halide⁶. This strategy works well for small alkyl groups but larger groups are expected to react slowly (secondary halides) or possibly not at all (tertiary halides)⁷. Since the early investigations of imidazolium SDAs alternative synthetic methodologies have been developed for imidazolium salt synthesis driven by their suitability as N-heterocyclic carbene (NHC) precursors^{8, 9} as outlined in Scheme 2.1. The alternative synthetic methods enable a wider range of substituent groups to be synthesized. With established synthetic methods we were also interested if the same product specificity would be encountered with larger imidazolium SDAs.



Scheme 2.1: 1,3-disubstituted imidazolium synthesis

Layered silicate materials have been widely investigated as catalysts and adsorbents. This is best exemplified by the MCM-22 (MWW)¹⁰ family of molecular sieves. These materials contain layers in the as-made form that condense to a fully four-

connected framework upon calcination. Different inorganic compositions define other MWW materials (borosilicate ERB-1, aluminosilicate SSZ-25 and pure silica ITQ-1). Several other materials with less order have also been investigated and shown to be active catalysts for a variety of reactions (MCM-56 and ITQ-30 for example)^{11,12}. Another aspect of this family is the ability to modify the layered precursor to create a pillared material (MCM-36)¹³ and even a delaminated/exfoliated material (ITQ-2)¹⁴. The high external surface area of these materials has attracted attention due to the possibility of catalytic reactions occurring on the external surface with substrates too large to fit inside the pores of a regular zeolite. In addition to MWW, other layered precursor materials that convert to four-connected products have been reported. These include SSZ-71 (precursor to SSZ-42 (IFR))¹⁵ and CDS-1 (CDO)¹⁶.

The original SSZ-70 synthesis with 1,3-diisopropylimidazolium and boron required greater than two months heating at 150°C under fluoride conditions with this being reduced to 1–2 weeks without fluoride (at 170°C). Modest catalytic activity in acid catalyzed hydrocarbon reactions was reported in the original discovery. Post synthetic aluminum insertion was required for catalytic activity with the modest catalytic activity possibly due to incomplete Al-exchange¹⁷. Therefore, an exploration of guest/host relationships using an expanded imidazolium library was warranted with an objective to directly synthesize aluminum-containing SSZ-70. Also, product formation kinetics could be improved using an alternative SDA.

The SDAs selected were anticipated to show changes in product distribution that could offer insight into structural features of SSZ-70. Figure 2.1 presents the sixteen guest molecules studied. The SDA library shows variation in steric demand at the charge center

(**1**, **2**, **5** and **11** less sterically demanding), periodicity (**5** and **11** have larger spacing between substituent groups) and substituent rigidity (branched and cyclic alkyl groups to rigid bicyclic and tricyclic alkyl groups). In addition, aromatic substituent groups were explored using **14** and **16**. The organocations span a wide carbon to charge range of 5 to 27 representing moderately hydrophilic for 1,3-dimethylimidazolium **1** to very hydrophobic for 1,3-bis(1-adamantyl)imidazolium **15** and 1,3-bis(2,6-diisopropylphenyl)imidazolium **16**. The zeolite chemistry of 1,3-diisopropylimidazolium has been well documented but is included here for completeness. In addition, boron rich conditions were explored using 1,3-dimethyl- and 1,3-diethylimidazolium as both SDAs show strong selectivity to ZSM-22 (TON)³ under aluminosilicate and pure silica conditions. Many recently discovered large- and extra large pore zeolite topologies have employed organocations with $C/N^+ \geq 17$ (e.g. SSZ-24 (AFI), CIT-5 (CFI), ITQ-21, SSZ-53 (SFH) & SSZ-59 (SFN)). Generally these materials are synthesized under a narrow range of inorganic conditions with germanium required for ITQ-21 and low trivalent substitution (boron or aluminum) for the other one-dimensional products.

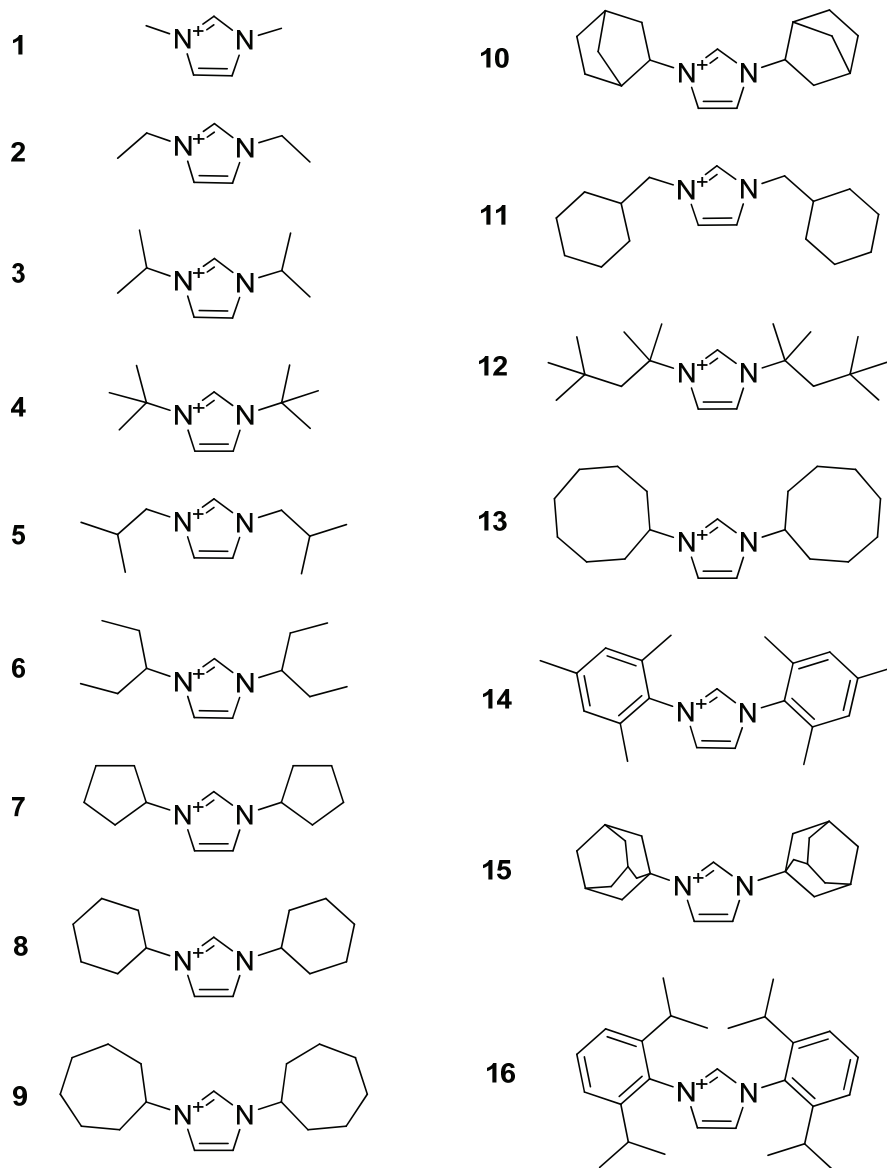


Figure 2.1: Imidazolium Structure Directing Agents Studied

As touched on above, inorganic reaction conditions play an important role in determining product formation. To study SSZ-70 formation five inorganic composition areas were investigated. The first was pure silica fluoride reactions where the water to silica ratio was varied from 3.5 to 14.5 in accordance with previous reports. Under

concentrated conditions beta is often produced (three dimensional large pore framework), with ZSM-12 (MTW, one dimensional large pore framework) a common product at high water to silica ratios. For these reactions low framework density products are favored at low water to silica ratios with higher framework densities emerging at high water to silica ratios. Second was borosilicate fluoride conditions modeled after those where SSZ-70 was originally discovered. Here the water to silica ratio was held constant around 15 and $\text{SiO}_2/\text{B}_2\text{O}_3$ varied. Low boron substitution at relatively high water to silica ratios could be expected to give similar phase selectivity to pure silica fluoride reactions at similar dilution (one-dimensional products favored). As more boron is incorporated into the reaction gel a transition to lower framework density phases (two or three dimensional) is possible. In addition borosilicate and aluminosilicate hydroxide reactions were explored. The product under borosilicate and aluminosilicate conditions is often different with the same guest molecule¹⁸. The reactions at silica to alumina (SAR) of 35 used sodium Y (FAU) zeolite as the aluminum source after the success in crystallizing SSZ-26¹⁹. Finally, the results from these four conditions were used to select SDAs for aluminosilicate fluoride reactions. The aluminosilicate fluoride reactions were performed at water to silica ratio of 15 with $\text{SiO}_2/\text{Al}_2\text{O}_3$ varied in accordance with the borosilicate fluoride reactions. All reactions were performed at 150°C in the initial reaction scheme. As described below, several reactions were repeated at 170 or 175°C to further explore the structure directing role of select guest molecules.

2.2: Experimental Section

2.2.1: Structure Directing Agent Synthesis

All reagents were purchased from commercial vendors and used as received. SDAs **1–3** were synthesized by quaternizing an imidazole with the appropriate alkyl halide⁶. 1,3-bis(2,4,6-trimethylphenyl)imidazolium chloride **14** (1,3-bis(mesityl)imidazolium chloride) and 1,3-bis(2,6-diisopropylphenyl)imidazolium chloride **16** were purchased from Sigma-Aldrich and used as received. All other SDAs were synthesized by adapting published procedures^{20, 21}. Crude tetrafluoroborate salts were purified by recrystallization. Similar recrystallization attempts for halide salts were largely unsuccessful, therefore, an aqueous activated carbon treatment was employed²². Liquid NMR spectra were recorded on 300 MHz Varian Mercury spectrometers. Combustion analysis was performed at the Chevron Energy Technology Center (Richmond, CA) using a Carlo-Erba Combustion Elemental Analyzer. All SDAs were exchanged to the hydroxide form using Dowex Monosphere 550A UPW hydroxide resin (Supelco). Final hydroxide concentration was determined by titration with 0.01N HCl solution to a phenolphthalein end point. Several reactions with 1,3-bis(cyclohexyl)imidazolium **8** and 1,3-bis(1-adamantyl)imidazolium **15** were performed with SDA⁺OH⁻ solutions obtained after ion-exchange from commercially available tetrafluoroborate salts (Sigma-Aldrich). Ion exchange of **15**·BF₄ took approximately one week at room temperature due to the low solubility of the parent salt (>90% ion exchange by titration).

1,3-dimethylimidazolium iodide (**1**): 1-methylimidazole (4.11g, 50 mmol, Sigma-Aldrich, 99%) in 50mL ethyl acetate (J.T. Baker, HPLC Grade) was cooled to 0°C in an ice bath. Once cool, iodomethane (7.77g, 54.7 mmol, Sigma-Aldrich, 99%) was added dropwise via addition funnel. The solution was allowed to warm slowly to room temperature. Stirring was continued for approximately 60 hours then the solution was filtered and the residue was washed with diethyl ether. The product dried under high vacuum overnight yielding 10.74g (47.9 mmol, 96% yield) of white solids (used without further purification). ¹H NMR (300 MHz, DMSO-d₆): 9.07, 7.70, 3.85. ¹³C NMR (75MHz, DMSO-d₆): 136.9, 123.4, 35.8. Analysis calculated for C₅H₉IN₂: C, 26.80; H, 4.05; N, 12.50 (C/N=2.14). Found: C, 26.90; H, 4.23; N, 12.31 (C/N=2.19).

1,3-diethylimidazolium iodide (**2**): 1-ethylimidazole (4.81g, 50 mmol, Sigma-Aldrich, 99%) in 50mL ethyl acetate was cooled 0°C in an ice bath. Once cool, iodoethane (8.69g, 55.7 mmol, Sigma-Aldrich, 99%) was added dropwise via an addition funnel. The solution was allowed to warm slowly to room temperature then stirred overnight. The precipitate was filtered off and washed with diethyl ether. The filtrate was collected and an additional 8.96g (57.4 mmol) iodoethane was added and stirring continued at room temperature for six days. The solution was filtered again and the residue was washed with diethyl ether. The combined solids were dried overnight under high vacuum yielding 9.76g white solids (38.7 mmol, 77% yield) that were used without further purification. ¹H NMR (300 MHz, DMSO-d₆): 9.25, 7.83, 4.20, 1.42. ¹³C NMR (75MHz, DMSO-d₆): 135.4, 122.1, 44.2, 15.1. Analysis calculated for C₇H₁₃IN₂: C, 33.35; H, 5.20; N, 11.11 (C/N=3.00). Found: C, 33.26; H, 5.29; N, 10.95 (C/N=3.04).

1,3-bis(*tert*-butyl)imidazolium tetrafluoroborate (**4**): *tert*-butylamine (7.32g, 100 mmol, Alfa-Aesar, 98%) in 100mL toluene (EMD, ACS Reagent) was placed in a room temperature water bath then paraformaldehyde (3.16g, 100 mmol, Fisher, 95%) was added with strong stirring. The solution was stirred at room temperature for 30 minutes then ice was added to the water bath. After cooling for one hour another 7.32g (100 mmol) *tert*-butylamine was added dropwise via addition funnel. Tetrafluoroboric acid (18.30g, 100 mmol, Alfa-Aesar 48 wt% in water) was diluted to 30wt% with 9.16g water then added dropwise via addition funnel. The ice bath was removed and the solution warmed for 30 minutes then glyoxal solution (14.488g, 100 mmol, Alfa-Aesar, 40 wt% in water) was added dropwise. The flask was heated at 40°C overnight then allowed to cool to room temperature. The solution was filtered and the residue washed with 50 mL water and 100 mL diethyl ether then dried overnight under high vacuum yielding 13.28g white solids (49.5 mmol, 50% yield) that were used without further purification. ¹H NMR (300 MHz, DMSO-d₆): 8.98, 8.05, 1.60. ¹³C NMR (75MHz, DMSO-d₆): 132.2, 120.5, 59.6, 29.1. Analysis calculated for C₁₁H₂₁BF₄N₂: C, 49.28; H, 7.90; N, 10.45 (C/N=4.72). Found: C, 48.87; H, 8.18; N, 10.34 (C/N=4.73).

1,3-diisobutylimidazolium bromide (**5**): Isobutylamine (7.32g, 100 mmol, Alfa-Aesar, 99%) in 100mL toluene (EMD, ACS Reagent) was placed in a room temperature water bath then paraformaldehyde (3.16g, 100 mmol, Fisher, 95%) was added with strong stirring. The solution was stirred at room temperature for 30 minutes then ice was added to the water bath. Hydrobromic acid solution (16.87g, 100 mmol, Sigma-Aldrich, 48 wt%) was diluted to 20 wt% with 23.66g water then placed on ice for approximately one hour. After cooling the toluene solution for one hour another 7.32g (100 mmol) isobutylamine

was added dropwise via addition funnel. The cold hydrobromic acid solution was added dropwise via addition funnel. The ice bath was removed and the solution warmed for approximately two hours then glyoxal solution (14.52g, 100 mmol, Alfa-Aesar, 40 wt% in water) was added dropwise. The reaction was stirred at room temperature for approximately 36 hours. The solution was concentrated by rotary evaporation to give a viscous yellow/orange oil. Purification was achieved by adding 125 mL water and 20mL saturated KHCO_3 and extracting with diethyl ether (2x100 mL). The aqueous phase was treated with 1.55g activated carbon (Sigma-Aldrich) and stirred overnight at room temperature. The carbon was filtered off and washed with a small amount of water. This process was repeated three times until the filtrate was colorless to the eye. The filtrate was concentrated by rotary evaporation and the residue extracted with chloroform (2x100 mL) then filtered. The chloroform extracts were combined, dried over MgSO_4 , filtered and stripped down by rotary evaporation to give a waxy residue. Further drying under high vacuum yielded 20.57g off-white solids (78.7 mmol, 79% yield). ^1H NMR (300 MHz, DMSO-d_6): 9.41, 7.88, 4.06, 2.11, 0.85. ^{13}C NMR (75MHz, DMSO-d_6): 136.4, 122.8, 55.4, 28.7, 19.0. Analysis calculated for $\text{C}_{11}\text{H}_{21}\text{BrN}_2$: C, 50.58; H, 8.10; N, 10.72 (C/N=4.72). Found: C, 50.27; H, 8.23; N, 10.61 (C/N=4.74).

1,3-bis(pentan-3-yl)imidazolium bromide (**6**): Using 3-aminopentane (2x70 mmol, Alfa-Aesar, 98%) the procedure described for **5** was followed yielding 14.82g white solids (51.2 mmol, 73% yield). ^1H NMR (300 MHz, DMSO-d_6): 9.75, 8.10, 4.24, 1.84, 0.70. ^{13}C NMR (75MHz, DMSO-d_6): 135.2, 121.3, 64.0, 27.2, 9.9. Analysis calculated for $\text{C}_{13}\text{H}_{25}\text{BrN}_2$: C, 53.98; H, 8.71; N, 9.68 (C/N=5.58). Found: C, 53.69; H, 8.57; N, 9.51 (C/N=5.64).

1,3-bis(cyclopentyl)imidazolium tetrafluoroborate (**7**): Using cyclopentylamine (2x147 mmol, Alfa-Aesar, 99%) the procedure for **4** was followed. Unlike **4**, no solid precipitate was visible so layers were separated after adding 150 mL diethyl ether and 75 mL saturated NaHCO₃ solution. The top ether/toluene layer was discarded and the aqueous layer plus oily residue were extracted with chloroform (3x100 mL). Combined CHCl₃ extracts and washed with brine (100 mL), dried over MgSO₄, filtered and stripped down by rotary evaporation to obtain a dark, waxy residue. Further drying under high vacuum did not change the waxy residue. The residue was finely ground using a mortar and pestle then extracted with diethyl ether using a Soxhlet apparatus. The extracted solids were recrystallized from 4:1 tetrahydrofuran/ethyl acetate to give 16.09g light tan solids. Further purification using activated carbon treatment as described for **5** (added 80 mL water plus 30 mL ethanol to dissolve) yielded 15.33g light yellow solids (52.5 mmol, 36% yield). ¹H NMR (300 MHz, DMSO-d₆): 9.36, 7.90, 4.74, 2.23-2.16, 1.91-1.78, 1.75-1.63. ¹³C NMR (75MHz, DMSO-d₆): 134.6, 121.4, 60.6, 32.6, 23.2. Analysis calculated for C₁₃H₂₁BF₄N₂: C, 53.45; H, 7.25; N, 9.59 (C/N=5.57). Found: C, 55.54; H, 7.82; N, 10.00 (C/N=5.55).

1,3-bis(cyclohexyl)imidazolium tetrafluoroborate (**8**): Using cyclohexylamine (2x200 mmol, Alfa-Aesar, 98+%) the procedure for **4** was followed. The solid precipitate was filtered off and washed with 150 mL water then 150 mL diethyl ether and dried overnight under high vacuum. Recrystallization from 2:1 ethyl acetate/dichloromethane yielded 33.72g off-white solids after drying under high vacuum (105.3 mmol, 53% yield). ¹H NMR (300 MHz, DMSO-d₆): 9.19, 7.88, 4.24, 2.07-2.03, 1.84-1.62, 1.43-1.30, 1.24-1.15. ¹³C NMR (75MHz, DMSO-d₆): 133.5, 120.8, 58.8, 32.4, 24.6, 24.4. Analysis

calculated for $C_{15}H_{25}BF_4N_2$: C, 56.27; H, 7.87; N, 8.75 (C/N=6.43). Found: C, 56.56; H, 7.67; N, 8.68 (C/N=6.52).

1,3-bis(cycloheptyl)imidazolium bromide (**9**): Using cycloheptylamine (2x110.4 mmol, Alfa-Aesar, 97%) the procedure for **5** was followed yielding 23.60g white solids after drying under high vacuum (69.1 mmol, 63% yield). 1H NMR (300 MHz, DMSO- d_6): 9.44, 7.93, 4.50, 2.08–1.97, 1.95–1.97, 1.77–1.69, 1.65–1.56, 1.54–1.46. ^{13}C NMR (75MHz, DMSO- d_6): 133.5, 120.8, 61.1, 34.7, 26.8, 23.3. Analysis calculated for $C_{17}H_{29}BrN_2$: C, 59.82; H, 8.56; N, 8.21 (C/N=7.29). Found: C, 59.45; H, 8.33; N, 8.08 (C/N=7.36).

1,3-bis(bicyclo[2.2.1]heptan-2-yl)imidazolium bromide (**10**) (1,3-bis(norbornyl)imidazolium bromide): Using *exo*-2-aminonorbornane (2x19.1 mmol, Sigma-Aldrich, 99%) the procedure for **5** was followed yielding 3.69g off-white waxy solids (10.9 mmol, 57% yield). 1H NMR (300 MHz, DMSO- d_6): 9.39, 7.91, 4.38, 2.55, 2.39, 1.94–1.91, 1.62–1.50, 1.32–1.21. ^{13}C NMR (75MHz, DMSO- d_6): 134.1, 121.5, 62.4, 42.70, 42.68, 37.82, 37.79, 35.71, 35.11, 27.49, 26.31. Analysis calculated for $C_{17}H_{25}BrN_2$: C, 60.53; H, 7.47; N, 8.31 (C/N=7.28). Found: C, 60.23; H, 7.22; N, 8.20 (C/N=7.35).

1,3-bis(cyclohexylmethyl)imidazolium bromide (**11**): Using cyclohexanemethylamine (2x110.4 mmol, Alfa-Aesar, 98%) the procedure for **5** was followed yielding 26.57g off-white waxy solids (77.8 mmol, 70% yield). When performing the activated carbon treatment 250 mL water plus 50 mL methanol was used to dissolve the residue. 1H NMR (300 MHz, DMSO- d_6): 9.29, 7.82, 4.06, 1.79, 1.69–1.66, 1.52–1.48, 1.20–1.13, 0.99–0.91. ^{13}C NMR (75MHz, DMSO- d_6): 136.4, 122.8, 54.3, 37.5,

29.3, 25.6, 24.9. Analysis calculated for $C_{17}H_{29}BrN_2$: C, 59.82; H, 8.56; N, 8.21 (C/N=7.29). Found: C, 59.43; H, 8.35; N, 8.07 (C/N=7.37).

1,3-bis(2,4,4-trimethylpentan-2-yl)imidazolium tetrafluoroborate (**12**) (1,3-bis(isooctyl)imidazolium tetrafluoroborate): Using 2-amino-2,4,4-trimethylpentane (2x120 mmol, TCI America, 95%) the procedure for **7** was followed omitting Soxhlet extraction. Recrystallization from dichloromethane/tetrahydrofuran yielded 11.76g off-white solids (30.9 mmol, 26% yield). 1H NMR (300 MHz, DMSO- d_6): 9.19, 8.13, 1.95, 1.66, 0.79. ^{13}C NMR (75MHz, DMSO- d_6): 133.5, 120.9, 62.8, 52.7, 31.3, 30.3, 29.3. Analysis calculated for $C_{19}H_{37}BF_4N_2$: C, 60.00; H, 9.81; N, 7.37 (C/N=8.14). Found: C, 61.38; H, 9.94; N, 7.50 (C/N=8.18).

1,3-bis(cyclooctyl)imidazolium bromide (**13**): Using cyclooctylamine (2x98.3 mmol, Alfa-Aesar, 97+%) the procedure for **5** was followed yielding 20.315g off-white solids (55.0 mmol, 56% yield). Similar to **11**, methanol was added during the activated carbon treatment to dissolve the residue. 1H NMR (300 MHz, DMSO- d_6): 9.50, 7.91, 4.56, 2.01–1.87, 1.67–1.55. ^{13}C NMR (75MHz, DMSO- d_6): 133.8, 120.9, 60.2, 32.3, 26.1, 24.9, 23.2. Analysis calculated for $C_{19}H_{33}BrN_2$: C, 61.78; H, 9.00; N, 7.58 (C/N=8.15). Found: C, 63.93; H, 9.79; N, 7.99 (C/N=8.00).

1,3-bis(1-adamantyl)imidazolium bromide (**15**): An aqueous solution of 1-adamantylamine hydrochloride (Alfa-Aesar, 99%) was treated with potassium hydroxide and extracted with toluene, dried over Na_2SO_4 , filtered and stripped down by rotary evaporation to give 30.3g 1-adamantylamine (200 mmol). The procedure for **5** was followed except the reaction was heated at 45°C overnight yielding 26.23g white solids (62.8 mmol, 63% yield). When performing the activated carbon treatment 2:1

water/absolute ethanol was used to dissolve the residue. ^1H NMR (300 MHz, CD_3OD): 9.02, 7.94, 2.27, 1.91, 1.85. ^{13}C NMR (75MHz, CD_3OD): 132.2, 120.6, 61.4, 43.4, 36.4, 31.0. Analysis calculated for $\text{C}_{23}\text{H}_{33}\text{BrN}_2$: C, 66.18; H, 7.97; N, 6.71 (C/N=9.86). Found: C, 62.37; H, 8.26; N, 6.44 (C/N=9.68).

2.2.2: Inorganic Reactions

All reactions were performed in 23 mL or 45 mL PTFE-lined stainless steel autoclaves (Parr Instruments). Hydroxide mediated reactions were tumbled at approximately 40 rpm using spits built into convection ovens. Fluoride mediated reactions were not tumbled. Silica sources were tetraethylorthosilicate (TEOS, Sigma-Aldrich, 98%) for fluoride reactions and Cab-O-Sil M5 fumed silica (Cabot) for hydroxide reactions. Boric acid (J.T. Baker, ACS Reagent) was used for borosilicate reactions and Reheis F-2000 (50–53 wt% Al_2O_3) or Na-Y zeolite (Tosoh HSZ-320NAA) were used in aluminosilicate reactions. Germanosilicate reactions used germanium dioxide (99.98%, Alfa-Aesar) and TEOS.

Gels for fluoride reactions were prepared by adding boric acid or aluminum hydroxide gel (if required) to the SDA^+OH^- solution then adding TEOS. The vessel was covered and stirred overnight to ensure complete TEOS hydrolysis then left uncovered in a 40°C oven to evaporate the required water and ethanol. Once the desired mass had been reached 48 wt% hydrofluoric acid (Mallinckrodt) was added with care and the gel stirred to form a stiff paste. The autoclave was sealed and placed in a 150°C (or 175°C) oven and opened every 7–10 days to assess reaction progress. After homogenizing, a small sample

was dispersed in 10 mL water and inspected under an optical microscope. For certain reactions at $\text{H}_2\text{O}/\text{SiO}_2=7.5$ and 14.5 small crystals were often visible. If no clear sign of crystallinity could be seen by optical microscope a small sample was filtered periodically and the XRD pattern inspected. All reactions were monitored to at least 60 days with the product labeled amorphous if no crystalline material was observed.

Gels for hydroxide reactions were prepared by adding water, 1N sodium hydroxide solution (if required), boron or aluminum source then silica and homogenizing by hand. Borosilicate reactions were run at $\text{SiO}_2/\text{B}_2\text{O}_3=8$ with no alkali hydroxide (gel composition 1.0 SiO_2 :0.125 B_2O_3 :0.25 SDA^+OH^- :23 H_2O); and the remaining reactions added sodium hydroxide with slightly increased water content (gel composition 1.0 SiO_2 :x B_2O_3 :0.20 SDA^+OH^- :0.10 NaOH :30.0 H_2O where $0.00 \leq x \leq 0.02$). Aluminosilicate reactions with NaY at SAR=35 had gel composition 1.0 SiO_2 :0.029 Al_2O_3 :0.20 SDA^+OH^- :y NaOH :30.0 H_2O where $y=0.25$ or 0.05 (except where NaOH content was varied in a separate series). The remaining reactions used unstructured Reheis F-2000 aluminum hydroxide gel as aluminum source with gel composition 1.0 SiO_2 :z Al_2O_3 :0.20 SDA^+OH^- :0.10 NaOH :30.0 H_2O with $z=0.02$ or 0.01. Finally, several germanosilicate reactions were performed with gel composition 1.0 SiO_2 :0.11 GeO_2 :0.5 SDA^+OH^- :3.5 H_2O at 170°C^{23} (not tumbled).

Reactions at 150°C were monitored every four to six days by measuring solution pH and looking for signs of phase separation (checked every two days for 170°C reactions). The reactions were checked until a pH maximum was observed then filtered. If no pH maximum was observed the reaction was continued until a sustained pH decline was observed (indicating SDA degradation). Several reactions at $\text{SiO}_2/\text{B}_2\text{O}_3=8$ formed a stiff paste that was not amenable to pH measurement. These reactions were stopped after 45

days heating and filtered as for other reactions. All crude products were washed with water plus a small amount of acetone and methanol then dried at room temperature. N,N-dimethylformamide (DMF) extractions were performed on as-made materials using ~0.4g zeolite : 10mL DMF. Solutions were sealed inside PTFE autoclaves and heated at 150°C for 24 hours. The extracted product was filtered and washed extensively with water then dried at room temperature.

2.2.3: Product Characterization

Powder X-ray diffraction (XRD) patterns were collected on a Scintag XDS-2000 diffractometer using $\text{CuK}\alpha$ radiation or Siemens D-500 diffractometer. Thermogravimetric analysis (TGA) was performed with a Netzsch STA449C using 75 mL min^{-1} air plus 25 mL min^{-1} Argon at a heating rate of 5°C min^{-1} . Nitrogen adsorption/desorption isotherms were collected on a Micromeritics ASAP 2000 instrument at 77K. Micropore volumes were calculated using the t-plot method. Solid-state NMR spectra were collected using either Bruker Avance 200 MHz or Bruker DSX 500 MHz instruments. ^{29}Si Bloch Decay (BD) experiments on as made materials used 500s recycle delay. Scanning electron microscopy (SEM) was performed using a JEOL JSM-6700F instrument. Elemental analyses were performed by Galbraith Laboratories (Knoxville, TN).

2.2.4: Catalytic Testing

Catalytic activity of aluminum containing SSZ-70 (Al-SSZ-70) materials was evaluated through the Constraint Index test (CI test)²⁴. Al-SSZ-70 synthesized using NaY as aluminum source was treated with 1N HCl at 95°C for 48 hours to neutralize any residual material that may affect catalytic activity²⁵. SSZ-25 was synthesized as previously described²⁶. All materials were calcined to 540°C at a heating rate of 1°C min⁻¹ under flowing nitrogen with a small amount of air. Calcined materials were ion-exchanged with 1N NH₄NO₃ at 50°C then filtered and washed with distilled de-ionized water. The ammonium-exchanged materials were pelletized, crushed and sieved with the 20–40 mesh fraction collected. Sized material (typically 0.5 g) was loaded into a stainless steel reactor tube supported by glass wool and activated by heating under flowing Argon at 350°C for at least four hours. Reactions were performed at 350°C unless otherwise noted. Hydrocarbon cracking was performed by introducing an equimolar n-hexane/3-methylpentane mixture (both from Sigma-Aldrich, ≥99.9%) via syringe pump into a mixing assembly with 5% Ar in He sweep gas (Airliquide, 99.999%) (LHSV=1.67 hr⁻¹). Products were analyzed using online GC/MS (Agilent GC 6890/MSD 5973N) with a Plot-Q capillary column.

2.3: Results and Discussion

2.3.1: Results Overview

The phases obtained from the initial inorganic reaction screen at 150°C are presented in Tables 2.1–2.4. Pure silica fluoride results in Table 2.1 show a cluster of SSZ-70 with **5** and **7-10**. This was surprising as fluoride mediated reactions typically produce products with very few silanol defects yet here we have a layered material with a high density of Q₃ silicon atoms (verified by ²⁹Si MAS and ²⁹Si CP-MAS NMR). Beta and ZSM-12 (MTW) appear frequently, with beta particularly common at H₂O/SiO₂=3.5. Both of these observations are consistent with recent reports under similar inorganic conditions^{2, 5}. Interestingly, no entry shows SSZ-70 across all dilutions. The entry for bis(cyclopentyl) SDA **7** at H₂O/SiO₂=14.5 displayed a transition from layered SSZ-70 plus EU-1 (EUO) at 52 days to EUO plus minor SSZ-70 upon further heating to 72 days. The intermediate dilution reaction was also heated to 72 days with only SSZ-70 present.

In addition to **1-3**; **6**, **13** and **15** produce the same product at all dilutions. These results extend the rare behavior of imidazolium SDAs in this chemistry where the organic influences nucleation selectivity to a greater extent than the fluoride anion. Previous reports with **3** and 1,2,3-trimethylimidazolium SDA showed product formation rates were influenced by dilution when the same product formed at all dilutions⁵. Similar trends were observed using **6**, **13** and **15** in the present study. Product formation tended to be slower than reported for the smaller imidazolium SDAs. For example, CFI and Beta, respectively, were observed after > 40 days heating at H₂O/SiO₂=3.5 using **15** and H₂O/SiO₂=14.5 using

13. In the low water to silica reactions fluoride is often found stabilizing double four ring (D4R) silicate units: none of the products obtained at $H_2O/SiO_2=3.5$ with known structures contain D4Rs (TON, MTT, BEA, MTW and CFI). The smaller 1,2,3- and 1,3,4-trimethylimidazolium SDAs make ITQ-12 (ITW) in the presence of fluoride or germanium^{5, 27}. ITW contains linked D4R units forming cavities with 8MR openings. Larger imidazolium SDAs would not fit in the ITW cage thereby removing this as a potential host. In the case of fluoride stabilizing D4R units the compensating charge from the SDA must be located relatively close. For imidazolium SDAs the charge is located at the center with symmetrical groups on either side in the present study. This feature adds a periodicity restriction to D4R spacing and may explain why no Beta Polymorph C (BEC) was observed as a minor component (ITQ-10 or ITQ-14 type materials)²⁸.

Table 2.1: Phases obtained from pure silica fluoride reactions at 150°C

SDA	H ₂ O/SiO ₂		
	3.5	7.5	14.5
1	ZSM-22	ZSM-22	ZSM-22
2	ZSM-22	ZSM-22	ZSM-22
3	ZSM-23	ZSM-23	ZSM-23
4	Beta	Beta	Amorphous
5	SSZ-70	SSZ-70	ZSM-12
6	ZSM-12	ZSM-12	ZSM-12
7	Beta	SSZ-70	SSZ-70→EU-1 ^a
8	Beta	SSZ-70	SSZ-70
9	Beta	SSZ-70	SSZ-70
10	NR ^b	SSZ-70	NR
11	Beta	Beta	ZSM-12
12	Amorphous	Amorphous	Amorphous
13	Beta	Beta	Beta
14	Amorphous	Amorphous	Amorphous
15	CIT-5	CIT-5	CIT-5
16	Amorphous	NR	NR

^a Initial product SSZ-70 plus EU-1 that transformed with extended heating to EU-1 plus SSZ-70

^b NR indicates synthesis not run

Three molecules did not make any product in the pure silica reactions. These were bis(isooctyl) SDA **12**, bis(mesityl) SDA **14** and bis(diisopropylphenyl) SDA **16**. Gels using **14** and **16** became yellow while evaporating water and ethanol. No other gels showed similar behavior. Reported pK_a values for 1,3-disubstituted imidazoliums in dimethylsulfoxide (DMSO) indicate phenyl substitution lowers C(2) proton pK_a by approximately 2 units compared to alkyl and benzyl substitution²⁹. In addition, kinetic H/D

exchange measurements in methanol gave significantly faster rates with mesityl and 2,6-diisopropylphenyl substitution³⁰. These data suggest phenyl substituted imidazoliums may be unstable due to enhanced attack at the acidic C(2) position. In comparison, **12** should possess similar C(2) proton acidity to the remaining 13 SDAs and therefore the inability to nucleate a crystalline phase was due to other factors. With no success in pure silica fluoride reactions these three SDAs were omitted from the borosilicate fluoride and hydroxide reactions to preserve the relatively limited supply. Further experiments in aluminosilicate hydroxide reactions will be discussed below.

The results for borosilicate reactions presented in Tables 2.2 and 2.3 show SSZ-70 as a very common product. The only SSZ-70 absences occur for **1**, **2**, **4**, **13** & **15**. SDA **4** does not crystallize any products except under concentrated fluoride conditions. SDA **6** shows strong specificity to MTW products with only one instance of SSZ-70 under high boron substitution with fluoride. In the absence of fluoride no crystalline product was obtained at the boron-rich condition studied. Bis(cyclooctyl) SDA **13** did not give any SSZ-70 products, with Beta the only zeolite product. This sharp delineation between the bis(C7) substituted SDAs **9-11** and bis(C8) substituted **13** could indicate SSZ-70 contains a feature that cannot accommodate the larger cyclooctyl group. MWW contains a sinusoidal 10MR within the layers and this apparent size exclusion suggests a similar feature may be present in SSZ-70. However, caution must be exercised as kinetic rather than thermodynamic factors largely determine what product evolves. Layered phases other than SSZ-70 were observed in borosilicate hydroxide reactions. Kanemite was found in several reactions with characteristic XRD reflections at 20–23 (broad) and 36°2 θ . In addition, an unidentified layered phase was observed with **15** with quite sharp XRD reflections less than

6°2θ and weaker reflections at higher diffraction angles. These reflections did not persist after calcination. Approximately 30 wt% mass loss >200°C was measured by TGA leading to the conclusion of a layered phase.

Table 2.2: Phases obtained from borosilicate fluoride reactions at 150°C

SDA	SiO ₂ /B ₂ O ₃	
	36	11
1	NR	ZSM-22
2	NR	ZSM-5
3	Amorphous + SSZ-70	Amorphous
4	Amorphous	Amorphous
5	SSZ-70	SSZ-70
6	ZSM-12	SSZ-70 ^a
7	SSZ-70	SSZ-70
8	SSZ-70	SSZ-70
9	SSZ-70	SSZ-70
10	NR	SSZ-70
11	SSZ-70	SSZ-70
13	Amorphous	Beta
15	CIT-5	Amorphous

^a Low angle reflections shifted compared to typical SSZ-70 product.

In contrast to the fluoride reactions with bis(adamantyl) SDA **15**, no zeolite phases were obtained in borosilicate hydroxide reactions. The original CIT-5 synthesis used LiOH to suppress SSZ-24 formation³¹, therefore, two further experiments were performed under pure silica and SiO₂/B₂O₃=100 conditions with NaOH replaced by LiOH. The reactions

were run statically at 165°C and CFI was obtained from both conditions (some layered material was present in the pure silica product). Boron rich fluoride and hydroxide reactions with **2** gave ZSM-5 (MFI). This SDA shows strong structure direction to TON materials under pure silica and aluminosilicate hydroxide conditions. Introducing sufficient boron to the gel induced a transition to three-dimensional MFI. Similarly, borosilicate reactions with **3** gave MTW at intermediate boron incorporation contrasting with SSZ-70 and MTT under boron rich and pure silica conditions, respectively.

Table 2.3: Phases obtained from borosilicate hydroxide reactions at 150°C

SDA	SiO ₂ /B ₂ O ₃			
	8	50	100	∞
1	Amorphous	NR	NR	ZSM-22 ³
2	ZSM-5	NR	NR	ZSM-22 ³
3	SSZ-70 ^a	ZSM-12	ZSM-12	ZSM-23 ³
4	Amorphous	Kanemite	Kanemite	Kanemite
5	SSZ-70	SSZ-70	SSZ-70	ZSM-12+SSZ-70
6	Amorphous	ZSM-12	ZSM-12	ZSM-12
7	SSZ-70	SSZ-70	SSZ-70	SSZ-70
8	SSZ-70	SSZ-70	SSZ-70	SSZ-70
9	SSZ-70	SSZ-70	SSZ-70	SSZ-70
10	NR	SSZ-70	NR	SSZ-70
11	SSZ-70 + Beta	SSZ-70	ZSM-12	ZSM-12
13	Beta	Beta	Beta	Quartz+Kanemite
15	Amorphous ^b	Layered ^c	Kanemite ^d	Layered ^{c,d}

^a Reaction at 170°C

^b SiO₂/B₂O₃=12

^b Sharp XRD reflections <6°2θ that do not persist on calcination

^c CFI obtained using LiOH instead of NaOH

The phases obtained from aluminosilicate reactions also reveal several SSZ-70 instances, again SDAs 5 & 7–10 show at least one occurrence for each reaction. Beta appears frequently throughout, with few instances of MTW. The first reaction with NaY as

aluminum source ($y=0.25$) shows Mordenite (MOR) appearing in all but one reaction. In an attempt to avoid MOR formation the lower NaOH condition was tried ($y=0.05$). Several interesting products were obtained with SSZ-70 observed using **7-10** and SSZ-16 (AFX) with the large bis(adamantyl) SDA **15**. Most reactions did not fully convert the NaY reagent with minor reflections visible by XRD. In comparison, the reactions using unstructured Reheis F-2000 show only three instance of SSZ-70. These data reinforce the subtle changes in nucleation selectivity brought about by inorganic reagent selection. An additional experiment using Reheis F-2000 at SAR=35 and NaOH/SiO₂=0.05 using **8** gave Beta.

Table 2.4: Phases obtained from aluminosilicate hydroxide syntheses at 150°C

SDA	$\text{SiO}_2/\text{Al}_2\text{O}_3$			
	35 (y=0.25)	35 (y=0.05)	50	100
3	ZSM-23	ZSM-23	ZSM-23	ZSM-23
4	MOR	Amorphous (NaY)	Amorphous	Amorphous
5	Beta (MOR)	ZSM-12 (NaY)	SSZ-70	SSZ-70
6	ZSM-12 (MOR)	ZSM-12 (NaY)	Amorphous	ZSM-12+amorphous
7	Beta	SSZ-70 + Beta	Beta	Beta+SSZ-70
8	Beta (MOR)	SSZ-70 (NaY/MOR)	Beta	Beta
9	Beta (MOR)	SSZ-70	Beta	Beta
10	NR ^a	SSZ-70 + Beta	NR	Beta
11	Beta+MOR (NaY)	ZSM-12 (NaY)	Beta	Beta
12	Magadiite (NaY)	Amorphous (NaY) ^c	NR	Amorphous
13	Beta (MOR)	Beta (NaY)	Beta	Beta
14	NR	Amorphous ^c	NR	NR
15	MOR	SSZ-16 (NaY)	Amorphous	SSZ-35
16	NR	Amorphous ^c	NR	NR

^a Phases in parentheses indicate minor impurity.

^b NR indicates reaction was not run.

^c NaOH/SiO₂=0.10.

To investigate the possibility of SSZ kinetic metastability the reaction screen was repeated for several conditions using SDAs **5**, **8** and **9**. Pure silica fluoride reactions were

repeated at 175°C and hydroxide reactions at 170°C. Pure silica fluoride and hydroxide results are presented in Tables 2.5 and 2.6 respectively. Higher temperature narrowed the SSZ-70 window for **5** and **8** with MTW and EUO observed at $H_2O/SiO_2=7.5$ and 14.5 respectively. In addition, Beta and SSZ-70 were observed in the concentrated reaction using **5**. The borosilicate hydroxide reactions with **5** gave MTW in all cases in contrast to the 150°C results where SSZ-70 was observed with boron substitution. These data indicate additional thermal energy was sufficient in several cases to produce a fully four-connected host product.

Table 2.5: Phases obtained from pure silica fluoride syntheses at 175°C

SDA	H_2O/SiO_2		
	3.5	7.5	14.5
5	Beta + SSZ-70	ZSM-12	ZSM-12
8	Beta	SSZ-70	EU-1 (SSZ-70) ^a
9	Beta	SSZ-70	SSZ-70

^a Phases in parentheses indicate minor impurity.

Table 2.6: Phases obtained from hydroxide syntheses at 170°C

SDA	SiO_2/B_2O_3			SiO_2/Al_2O_3	
	50	100	∞	35 (y=0.05)	50
5	ZSM-12	ZSM-12	ZSM-12	SSZ-70+ZSM-12	SSZ-70+amorphous
8	SSZ-70	SSZ-70	SSZ-70	Beta + SSZ-70	Beta
9	SSZ-70	SSZ-70	SSZ-70	SSZ-70	Beta

Finally, the above results indicated bis(isobutyl) SDA **5** to be the most selective to SSZ-70. A small number of aluminosilicate fluoride reactions were performed with $H_2O/SiO_2=15.5$ and $SAR=30-70$ at $150^\circ C$. SSZ-70 was obtained at $SAR=30, 50$ & 70 (minor impurity in $SAR=70$ product). Similar reactions using bis(cyclohexyl) SDA **8** at $SAR=40$ gave Beta, in accordance with the hydroxide reactions at $SAR=50$ and 100 .

Several interesting trends were observed in the approximately 160 reactions detailed above. Producing the normally aluminum rich AFX with a large, hydrophobic SDA was surprising. Energy minimization calculations indicate the SDA nicely occupies the large AFT cage (not shown). As noted in the original SSZ-16 report, no organic is expected to occupy the smaller Gmelinite cage³². Another intriguing result was obtaining SSZ-35 (STF) with **15** in the $SAR=100$ reaction. STF contains 18 MR cages connected through 10MR windows suggesting the imidazolium sitting in the 10 MR with adamantyl groups occupying the larger cavities. This supports the observation of STF using a diquatery tropane SDA in a recent study²³. Furthermore, the tropane- C_4 -tropane SDA was one of the original molecules reported to synthesize SSZ-16 so it appears these two molecules have certain similarities that enable structure direction to the same products. An important aspect was whether the **15** was intact within each host framework. If the SDA degraded to a fragment containing a mono-adamantyl moiety this could be the actual organic species occluded. Mono-adamantyl N,N,N-trimethyl-1-adamantanammonium can synthesize a variety of high silica phases²⁵ although no syntheses of CFI, AFX or STF using this SDA have been reported. Solid-state ^{13}C CP-MAS NMR was performed and all three products gave similar resonances. The alkyl carbon resonances were easily detected whereas the imidazolium resonances were broad and weak. All spectra agree with the

SDA chloride salt as shown in Figure 2.2. These data indicate the SDA was occluded intact within each host phase.

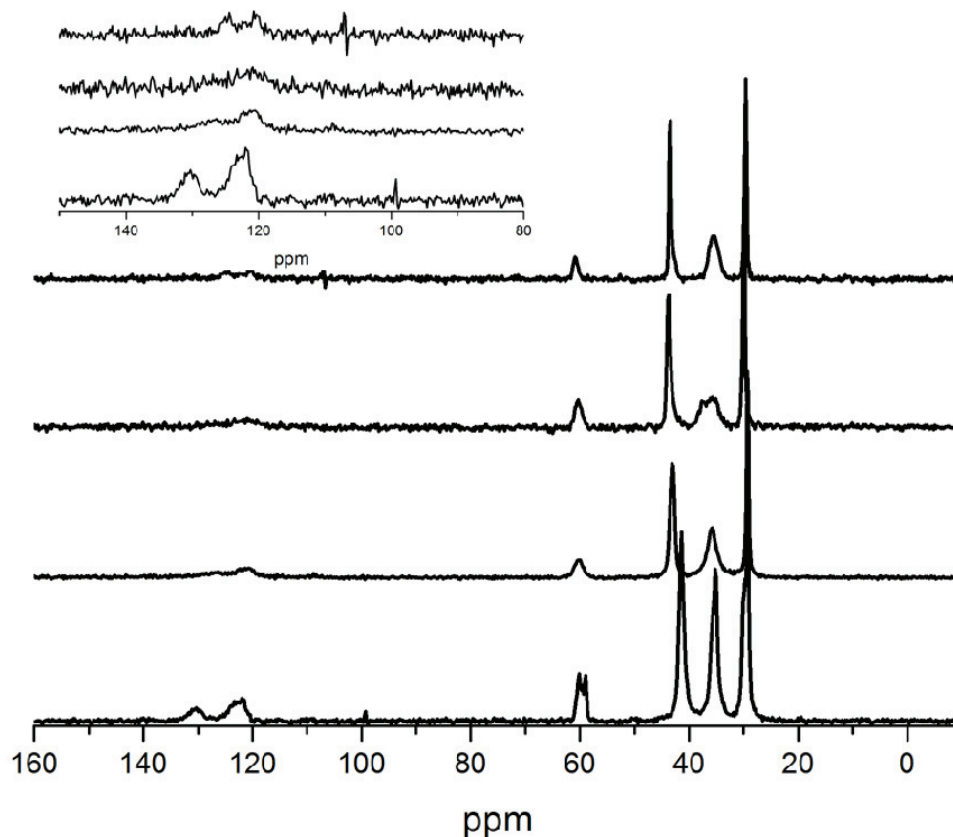


Figure 2.2: ^{13}C CP-MAS NMR of products obtained using 1,3-bis(1-adamantyl)imidazolium SDA **15**. Top to bottom=CIT-5, SSZ-35, SSZ-16 and SDA^+Cl^- . The inset enlarges the imidazolium region

Entries in Table 2.4 for **12**, **14** and **16** show no crystalline zeolite products in agreement with the previous pure silica fluoride results. Reactions with **14** and **16** rapidly discolored with viscous red oil appearing on the surface. Discoloration was attributed to degradation caused by the more acidic C(2) proton in these SDA and therefore no further reactions were performed. In addition, bis(*tert*-butyl) **4** only made MOR under sodium rich

NaY reaction conditions. MOR can be considered a default product given sufficient sodium and aluminum with nucleation and growth due to inorganic factors. Therefore, **4** should be included with **12** with both unable to direct the formation of any desirable phase. The inability of **4** to nucleate phases except under very narrow conditions of low water content was particularly puzzling. This SDA appeared an ideal candidate with intermediate hydrophobicity ($\Sigma(C+N)=13$) and similar periodicity to **3**. Additional NaY reactions and germanosilicate experiments were performed using **4**, **8**, **12** and **15** to gain further insight. The additional NaY reactions varied NaOH/SiO₂ to look for transitions to default products such as MOR. In addition, certain reactions looked at NaOH/SiO₂=0.10 and SDA⁺OH⁻/SiO₂=0.25. Here the total hydroxide content was higher and the SDA contributed a higher hydroxide ratio compared to silica. The results for these reactions are plotted in Figure 2.3 and show MOR appeared for all four SDAs. MOR was observed using **15** in the initial reaction screen so experiments at higher NaOH content were not performed. Layered Magadiite was observed with **12** for two reaction conditions with this eventually displaced by MOR at higher NaOH. Bis(cyclohexyl) SDA **8** shows four products with SSZ-70, Beta, MOR and NaP1 (GIS) forming from low to high NaOH content.

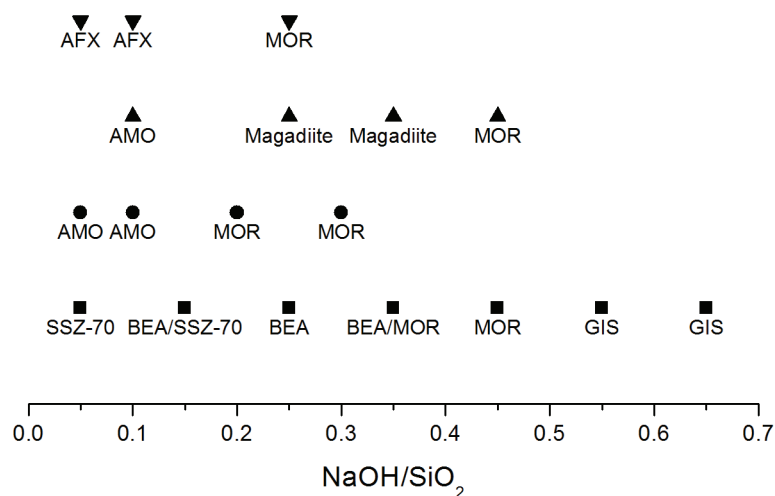


Figure 2.3: Phases obtained in NaY reactions as a function of NaOH/SiO₂ ratio for bis(cyclohexyl) SDA **8** (■), bis(*t*-butyl) SDA **4** (●), bis(isooctyl) SDA **12** (▲) and bis(adamantyl) SDA **15** (▼). AMO indicates amorphous and residual NaY is not shown

Germanosilicate reactions were investigated to see if D4R-rich structures could be produced. In this case a perturbation from the concentrated fluoride reaction results was anticipated. The results presented in Figure 2.4 show mostly amorphous material for **15** and **12** while **8** and **4** produced Beta, with ITQ-7 (ISV) visible for **4**. The gels for **12** and **15** formed solid masses that were difficult to probe. This was probably due to the low water content and hydrophobic SDAs. The smaller SDA **4** shows Beta plus ISV, with ISV containing D4R units, whereas regular Beta was observed with **8**. A possible explanation for these data is the smaller distance between adjacent charge centers in **4** compared to **8** as discussed earlier. Overall, the synthesis window for **4** was not enlarged and **12** did not succeed in nucleating a desirable crystalline phase. An insight to the relative inability of **4** and **12** to nucleate products was offered by crystallographic studies of NHC-Pd

complexes³³. These studies examined the excluded or buried volume associated with each NHC ligand and found bis(adamantyl) and bis(*tert*-butyl) ligands the most sterically demanding (highest buried volume). The local environment of **4**, **12** and **15** adjacent to nitrogen is similar with quaternary carbons in all three suggesting **12** should display similar steric demands. The methyl groups projected into the imidazolium plane by **4** and **12** may inhibit interaction with hydrated silica species thereby giving few or no products. This was supported by concentrated conditions being required for **4** to nucleate a crystalline phase with organic and silica species presumably in intimate contact with minimal solvent (water) present.

The steric factors discussed above appear contrary to the results obtained with **15** where three crystalline phases were obtained. However, if steric demand at the charge center was solely responsible for structure direction, minimal differences should be observed between the cycloalkyl substituted **7–9** and **12**. While some overlap does occur there are clear differences suggesting space filling away from the charge center is equally important. In this context the bulky, rigid adamantyl groups of **15** are a distinguishing feature. The adamantyl group offers favorable silicate interactions demonstrated by the number of high silica phases synthesized with mono-adamantyl SDAs. Therefore, obtaining three phases with **15** may be largely due to silicate organization away from the charge center. Both STF and CFI feature undulation along the pore with this being particularly pronounced in STF. The corrugated pores may give favorable interactions with the boomerang-shaped **15**. Also, SSZ-16 was only obtained from the NaY reaction, no product was synthesized at SAR=50 using unstructured aluminum hydroxide gel. The

Faujasite reagent contains many six-rings and this might help specify AFX containing exclusively six-rings.

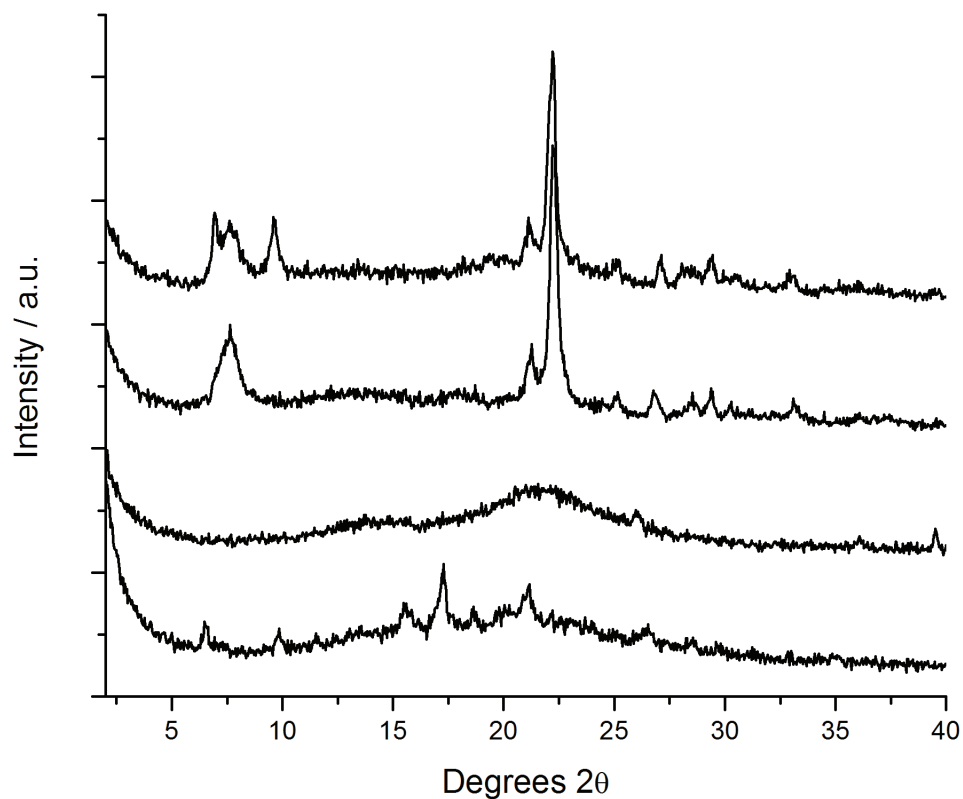


Figure 2.4: XRD patterns for germanosilicate reactions using **4**, **8**, **12** and **15**. Top to bottom=**4** (Beta+ISV), **8** (Beta), **12** (amorphous) and **15** (amorphous)

2.3.2: SSZ-70 Characterization

Powder XRD patterns are shown in Figures 2.5–2.7 for as-made and calcined SSZ-70. Preliminary inspection of the powder XRD pattern shows similarity to those of MWW precursor materials. Figure 2.5 shows XRD patterns for as-made Al-containing SSZ-70 synthesized in fluoride and hydroxide media using **5** (Al-SSZ-70(F) and Al-SSZ-70(OH)

respectively). Also included in Figure 2.5 is the XRD pattern of as-made SSZ-25 as a representative MWW material. Figure 2.6 enlarges the XRD patterns in the $2\text{--}12^\circ 2\theta$ range. The as-made pattern shows one reflection with large d-spacing ($\sim 27\text{\AA}$) and several integer multiples are also present. The pattern for Al-SSZ-70(OH) is considerably broader than both SSZ-25 and Al-SSZ-70(F) with the low angle reflection appearing as a weak shoulder. Broad reflections in the hydroxide material were likely due to smaller crystal size. All three materials give quite sharp reflections at $\sim 26.0^\circ 2\theta$ indicating similar structural features may be present in both materials. Inspection of the low-angle features in Figure 2.6 reveals enlarged d-spacing compared to MWW materials, similar to ITQ-30. Comparing the hydroxide and fluoride patterns reveals the same d-spacing for all reflections except one broad reflection at $\sim 8.7^\circ 2\theta$ for the fluoride product whereas the hydroxide product gives two reflections at ~ 7.9 and $9.5^\circ 2\theta$. This diffraction intensity difference could be due to differences in crystal size as observed in DIFFaX simulations of MCM-22 and MCM-56¹². Simulated diffraction patterns in this region were sensitive to the number of unit cells along the c-direction (orthogonal to layers) for 1–3 repeat units.

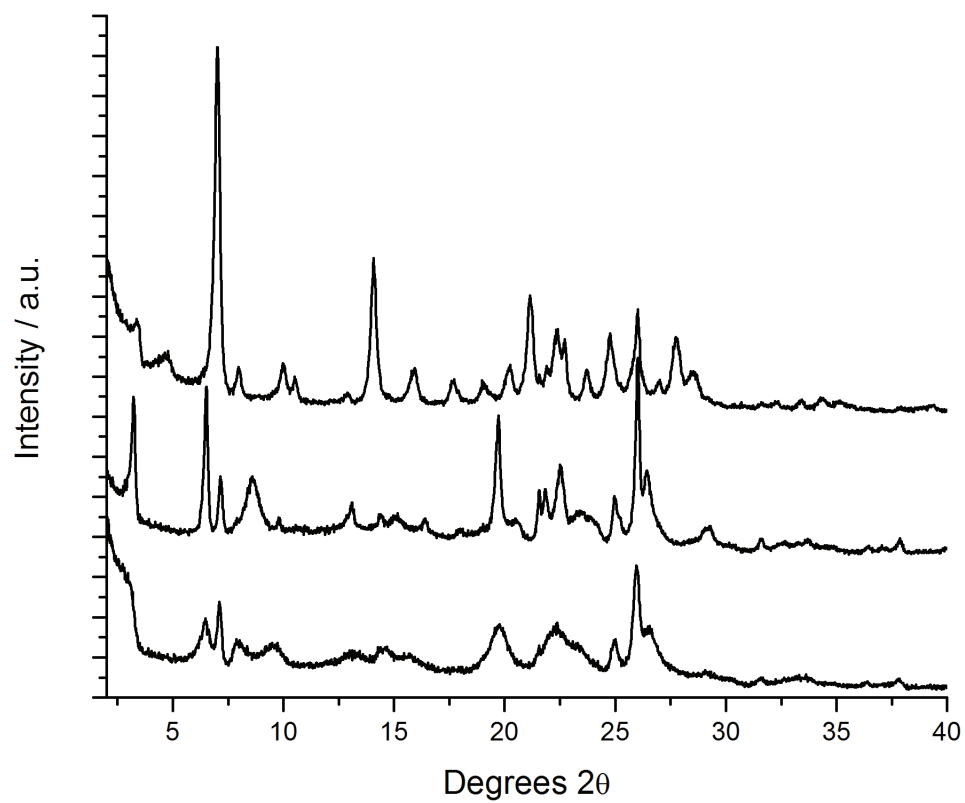


Figure 2.5: XRD patterns for top to bottom; SSZ-25, Al-SSZ-70 (F) and Al-SSZ-70 (OH)

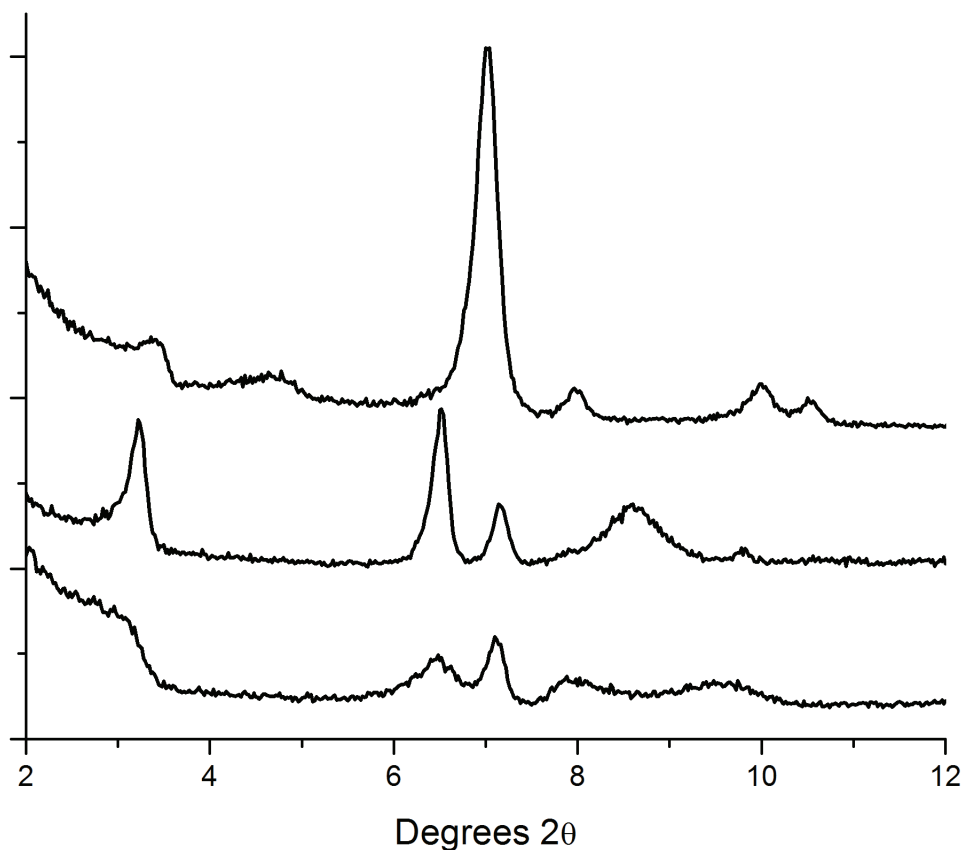


Figure 2.6: XRD patterns from 2–12°2θ for top to bottom; SSZ-25, Al-SSZ-70 (F) and Al-SSZ-70 (OH)

Figure 2.7 shows XRD patterns for calcined SSZ-70 materials synthesized in fluoride media using **5**. Shown are pure silica (Si-SSZ-70(F)), borosilicate (B-SSZ-70(F)) and aluminosilicate (Al-SSZ-70(F)) materials. For both Si-SSZ-70(F) and Al-SSZ-70(F) the two low-angle reflections present in the as-made material are absent or appear with reduced intensity after calcination. The first significant reflection occurs at 7.0°2θ (~12.5Å) in both materials. In contrast, the low-angle reflections persist after calcination for B-SSZ-70(F) albeit with lower relative intensity. Both low-angle reflections were not observed after calcining B-SSZ-70(OH).

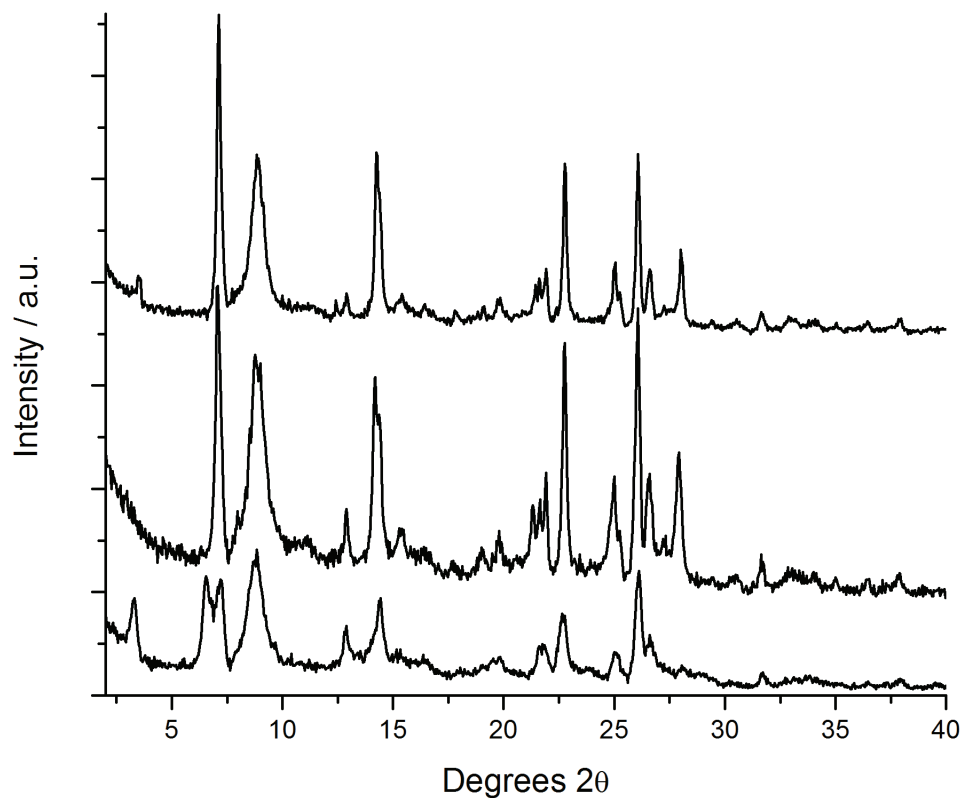


Figure 2.7: XRD patterns of calcined SSZ-70 products. Top to bottom; Si-SSZ-70(F), Al-SSZ-70 (F) and B-SSZ-70 (F)

Solid-state ^{29}Si NMR was performed on Si-SSZ-70 from fluoride and hydroxide reactions. Spectra were collected on samples obtained using bis(cycloheptyl) **9**. Figure 2.8 shows cross-polarization magic angle spinning (CP MAS) and Bloch decay (BD MAS) spectra on as-made Si-SSZ-70 samples. Both as-made spectra show significant Q^{32} silica content (-94 ppm resonance). A comparison of the CP and BD spectra show higher relative intensity for the -116 and -120 ppm resonances under CP conditions (2 ms contact time)

$^2 \text{Q}^n = \text{Si}(\text{OSi})_n(\text{OH})_{4-n}$

and relative decrease for the -106 ppm resonance. This change in relative intensity suggests SDA molecules do not reside in close proximity to the silicon resonating at -106 ppm. The resonances in the fluoride sample are well defined and span a similar chemical shift range to those reported for ITQ-1^{34, 35}. The calcined spectrum shown in Figure 2.9 shows six well resolved resonances with a small amount of Q³ silica still present. Tables 2.7 and 2.8 list the observed resonances for each sample studied as well as those reported for ITQ-1.

Table 2.7 gives the observed chemical shifts for as-made Si-SSZ-70 materials. Relative intensity was determined by integration of the BD MAS spectra. In general the resonances for Si-SSZ-70 samples were not as well resolved as those for ITQ-1. This was particularly true for the hydroxide sample. No attempt was made to deconvolute the spectra as the limited resolution did not warrant this. Therefore, fewer chemical shifts were included in the table. Inspecting the relative intensities shows a significant population of Q³ silica species in both hydroxide and fluoride samples. The resonance <-100 ppm for each sample can be assigned as Q³ but there was some ambiguity regarding the resonances near-105 ppm. The calcined spectrum for Si-SSZ-70(F) shown in Figure 2.9 clearly shows the -105 ppm resonance, whereas the -95 ppm one was significantly diminished. This suggests the -105 ppm resonance to be Q⁴ to give a relative Q³ abundance of ~10% in the as-made material. The broad resonance centered at -104 ppm for the hydroxide material could not be conclusively assigned to either Q³ or Q⁴ giving an estimated relative Q³ population of ~22–28%. The upper estimate for Q₃ content in the hydroxide sample was in general agreement with those reported for ITQ-1 (29–33%). For Si-SSZ-70(F) there was

no analogous material to compare the relative Q^3 population as fluoride reactions generally produce materials with very low defects (low Q^3).

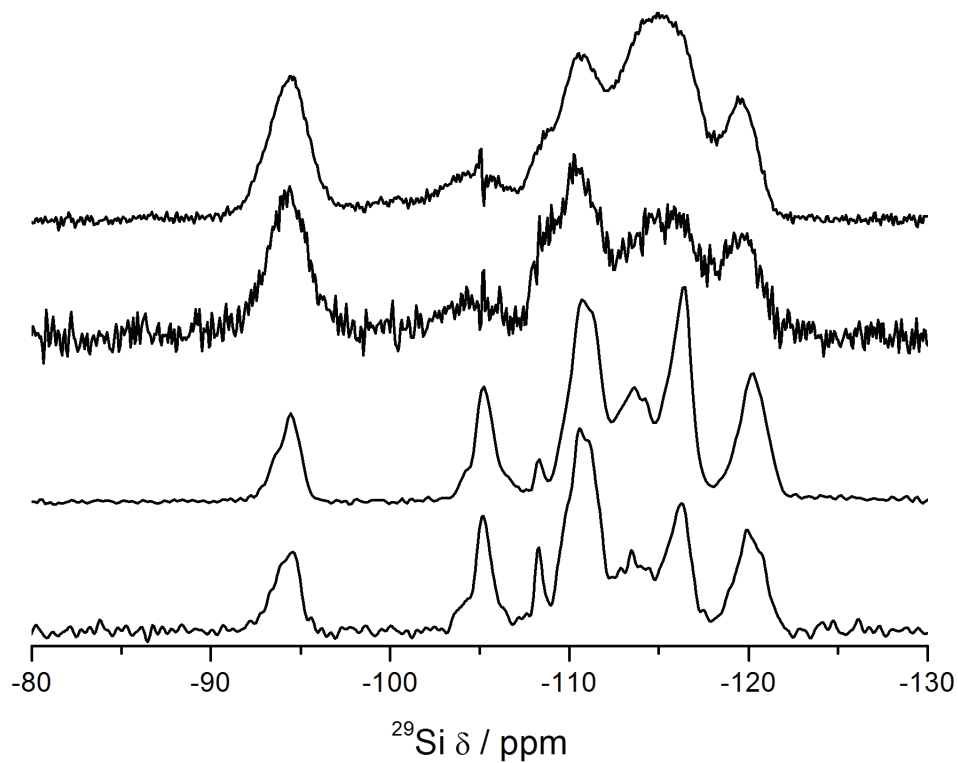


Figure 2.8: Solid-state ^{29}Si NMR spectra of Si-SSZ-70. Top to bottom: Si-SSZ-70(OH) CP-MAS, Si-SSZ-70(OH) BD-MAS, Si-SSZ-70(F) CP-MAS and Si-SSZ-70(F) BD-MAS

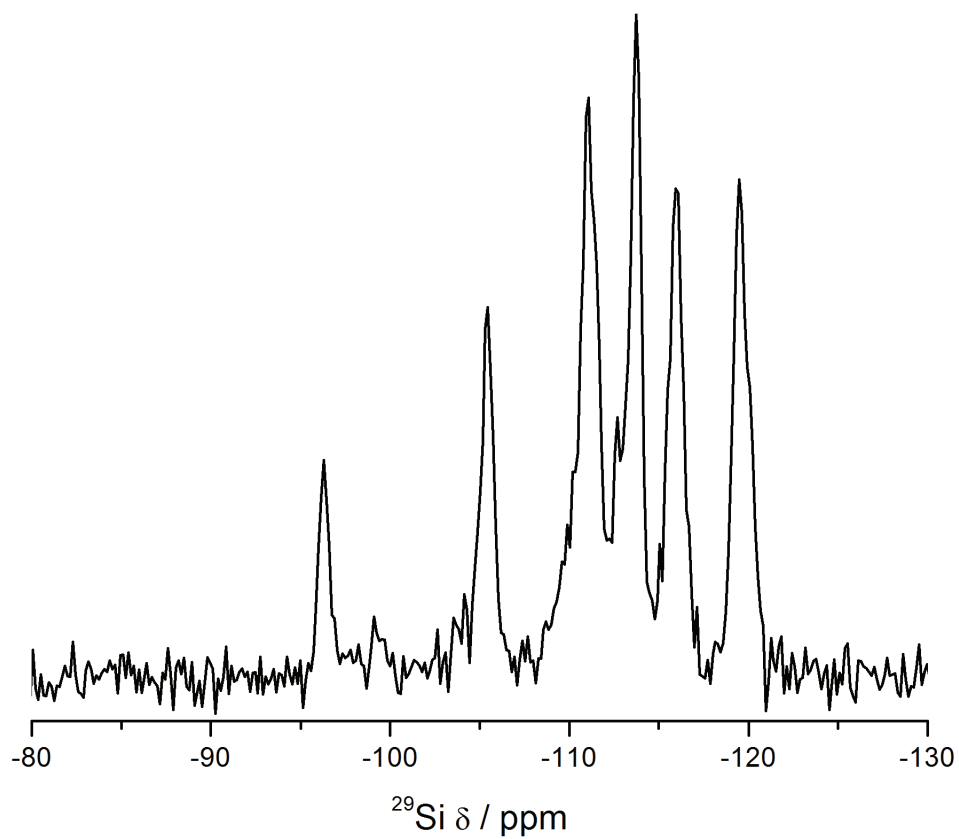


Figure 2.9: Solid-state ^{29}Si BD-MAS NMR of calcined Si-SSZ-70(F)

Table 2.7: ^{29}Si chemical shifts and relative intensities for as-made Si-SSZ-70(OH), Si-SSZ-70(F) and ITQ-1

Si-SSZ-70 (OH)		Si-SSZ-70 (F)		ITQ-1		
δ / ppm	<i>I</i> / %	δ / ppm	<i>I</i> / %	δ / ppm	Assignment	<i>I</i> / %
				-92.6	Q ³	12.0
-94.1	22.1	-94.6	10.5	-94.1	Q ³	19.0
-104.3	6.4	-105.2	11.5	-103.7	Q ³	1.9
-110.4	30.1	-108.3	4.9	-105.0	Q ⁴	2.8
-115.6	27.9	-110.6	30.5	-108.3	Q ⁴	1.7
-119.7	13.5	-113.5	12.1	-110.1	Q ⁴	27.8
		-116.3	15.6	-112.4	Q ⁴	2.5
		-119.9	14.8	-114.7	Q ⁴	10.7
				-116.7	Q ⁴	10.1
				-119.8	Q ⁴	11.5

Table 2.8: ^{29}Si chemical shifts and relative intensities for calcined Si-SSZ-70(F) and ITQ-

1

Si-SSZ-70 (F)		ITQ-1		
δ / ppm	<i>I</i> / %	δ / ppm	Assignment	<i>I</i> / %
-96.3	4.6			
-105.4	11.5	-105.9	Q ⁴	15.1
-111.0	25.9	-111.2	Q ⁴	15.1
-113.7	23.1	-111.8	Q ⁴	4.9
-116.0	17.3	-112.6	Q ⁴	7.6
-119.5	17.6	-113.9	Q ⁴	19.0
		-116.5	Q ⁴	18.9
		-120.3	Q ⁴	19.4

The chemical shifts and relative intensities for calcined Si-SSZ-70(F) shown in Table 2.8 show several differences. As mentioned above, calcination did not completely remove all Q³ species. In addition, the as-made resonance at -108.3 ppm was not visible in the calcined spectrum. It would appear unlikely that this resonance was from a silanol defect as the observed chemical shift is in the general range for Q⁴ silica. Also, ²⁹Si resonances of pentacoordinated silicon with fluorine are found in the -120 to -150 ppm range so the resonance should not arise from fluoride incorporation³⁶. This was supported by the weak shoulder at ~-108 ppm in the hydroxide spectra. The observed chemical shifts and relative intensities show similarity to those of ITQ-1.

SEM images of Si-SSZ-70(F) are shown in Figure 2.10. Thin hexagonal plates were visible in the as-made and calcined material. MWW materials form crystals with similar habit. The observed crystal habit supports the similarity to MWW materials as demonstrated by XRD and ²⁹Si NMR. Figure 2.11 shows a TEM image of B-SSZ-70 with the layers clearly observed. Images at higher magnification did not show pore features as observed for MCM-22¹⁰ and SSZ-25³⁷.

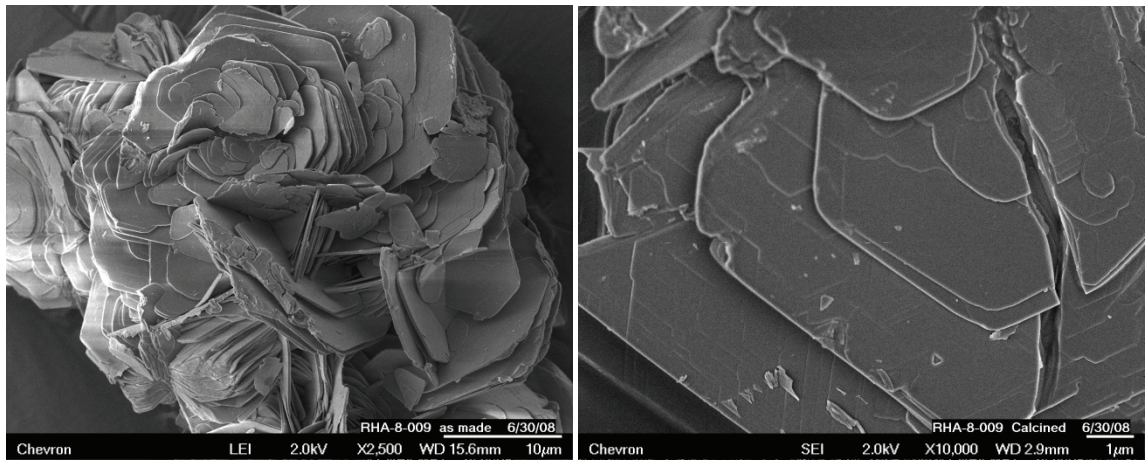
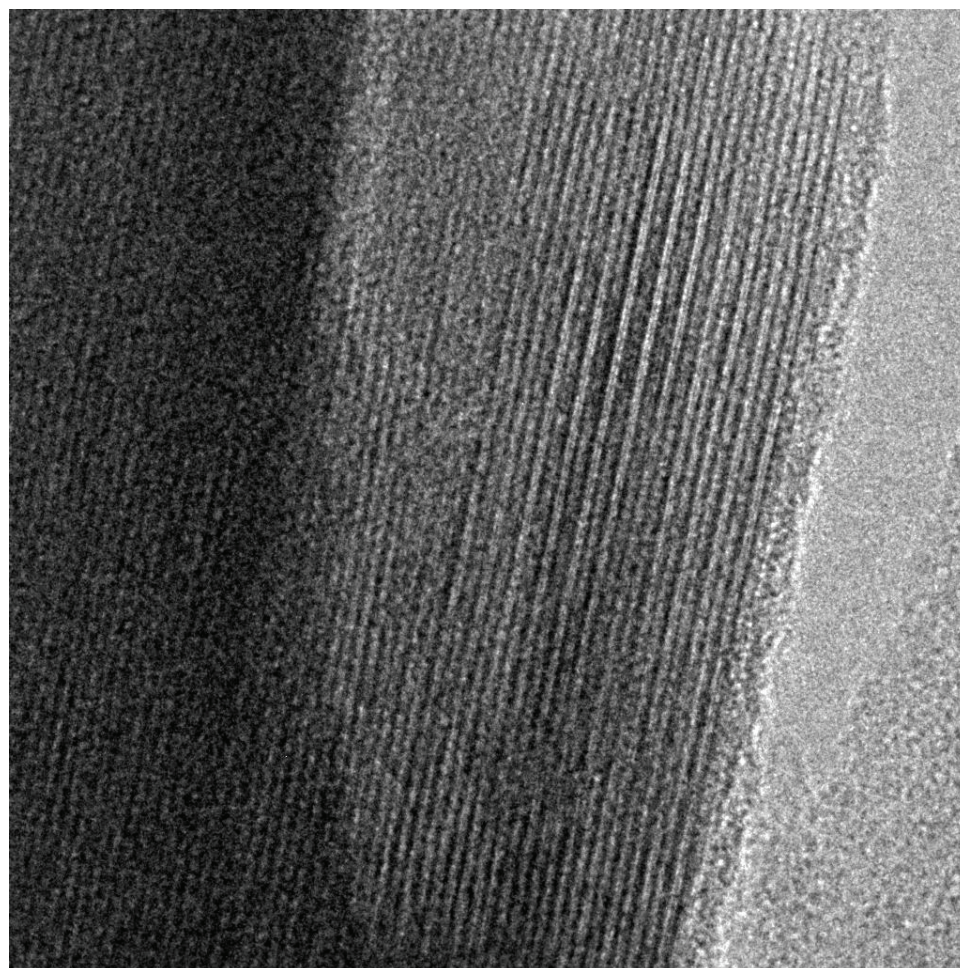


Figure 2.10: SEM images of as-made Si-SSZ-70 (left) and calcined Si-SSZ-70 (right)



SIZ16489 SSZ-70a
BC6Ebb 200kx

20 nm

Figure 2.11: TEM image of B-SSZ-70

Chemical analysis was performed on several products to gain further insight into SSZ-70. The majority of the chemical analysis was performed on SSZ-70 materials using **5**. One aspect of particular interest was the amount of fluoride incorporated into SSZ-70 materials. This was investigated through studying pure silica products as a function of water to silica ratio for **5**, **6** and **11**. These SDAs were chosen as **5** gave two instances of SSZ-70 plus MTW, **6** gave MTW under all three water to silica ratios and **11** transitioned

from Beta to MTW with increasing dilution. The phases for the nine products analyzed are restated in Table 2.9 for convenience.

Table 2.9: Phase summary for chemical analysis of pure-silica fluoride products using **5**, **6** and **11**

SDA	H ₂ O/SiO ₂ =3.5	H ₂ O/SiO ₂ =7.5	H ₂ O/SiO ₂ =14.5
5	SSZ-70	SSZ-70	MTW
6	MTW	MTW	MTW
11	Beta	Beta	MTW

Tables 2.10 and 2.11 present chemical analysis for pure silica fluoride products. The carbon and nitrogen data in Table 2.10 show less organic occluded within one-dimensional MTW compared to three-dimensional Beta. The measured organic content for SSZ-70 falls between these two boundaries. Calculated carbon to nitrogen ratios agree with those expected for the parent SDAs except **11** at H₂O/SiO₂=14.5 where 8.5 was observed (expected 7.3). This sample gave the lowest nitrogen content of all samples and therefore might contain higher relative error (0.5 wt% detection limit). Fluoride analysis for the same products is shown in Table 2.11. Calculated fluoride to nitrogen values is also included. All F/N ratios can be compared to the theoretical F/N value for the SDA⁺F⁻ salt (0.68 for all imidazolium SDAs studied). This value corresponds to a neutral product with no connectivity defects. The two SSZ-70 products show significantly lower fluoride content and F/N ratios compared to the other seven products. Fluoride absence means organic charge must be balanced by silanol defects³⁸ as observed by ²⁹Si NMR above. The remaining materials show F/N values very close to the theoretical value for defect-free

material. Two samples gave slightly higher ratios (0.83 and 0.86) with the 0.86 ratio calculated for the same MTW product using **11** that showed low nitrogen content above. Interestingly, the fluoride content of MTW products using **6** did not show a significant trend with water content. Previous studies using **3** found higher fluoride incorporation in MTT products with increasing water content⁵. Analysis reveals slightly higher fluoride content at $H_2O/SiO_2=3.5$ (~1.4 wt% and $F/N=0.83$) than the two other products (~1.0 wt% F and $F/N=0.7$). The $H_2O/SiO_2=3.5$ MTW product using **6** also shows slightly higher carbon and nitrogen content. The higher carbon, nitrogen and fluorine content suggest amorphous SiF_x species with occluded SDA might be present in small amounts (~1.7 wt% additional C+N).

Table 2.10: Carbon and nitrogen content for pure-silica fluoride products using **5**, **6** and

11

	$H_2O/SiO_2=3.5$			$H_2O/SiO_2=7.5$			$H_2O/SiO_2=14.5$		
SDA	C/wt%	N/wt%	C/N	C/wt%	N/wt%	C/N	C/wt%	N/wt%	C/N
5	11.91	2.41	4.9	13.65	2.79	4.9	6.94	1.43	4.9
6	9.71	1.67	5.8	8.14	1.39	5.9	8.17	1.43	5.7
11	15.46	1.99	7.8	13.72	1.74	7.9	7.28	0.86	8.5

Table 2.11: Fluoride content for pure-silica fluoride products using **5**, **6** and **11**

	$H_2O/SiO_2=3.5$		$H_2O/SiO_2=7.5$		$H_2O/SiO_2=14.5$	
SDA	F/wt%	F/N	F/wt%	F/N	F/wt%	F/N
5	0.69	0.29	0.83	0.30	1.06	0.74
6	1.38	0.83	0.99	0.71	1.02	0.71
11	1.46	0.73	1.25	0.72	0.74	0.86

Chemical analysis of B-SSZ-70(F), Al-SSZ-70(F) and Al-SSZ-70(OH) products synthesized using **5** in Table 2.12 show very similar organic content across the seven products. Carbon to nitrogen ratios were between 4.8 and 5.0 agreeing very well with the expected ratio of 4.7. Slightly higher fluorine content was measured in the borosilicate samples compared to the pure silica and aluminosilicate samples. With trivalent lattice substitution (B or Al) framework charge is introduced and fluoride is no longer required to balance the cation charge. However, the values calculated show little variation with lattice substitution for both boron and aluminum incorporation. In addition, the ratios for all three aluminosilicate samples were almost the same as the pure silica products. One report on MCM-22 synthesis using hexamethyleneimine with alkali fluoride salts showed varying amounts of fluoride incorporated in the aluminosilicate product³⁹. Under the approximately neutral reaction conditions the secondary amine should be protonated and similar cation/framework charge arguments must hold. Additional work is required to elucidate the exact nature of fluoride species present in B-SSZ-70(F) and Al-SSZ-70(F).

Inspecting the Si/B and Si/Al ratios measured in the as-made products reveals less boron incorporation than present in the reactions gel. Aluminosilicate fluoride and hydroxide products showed Si/Al ratios almost identical to the reaction gel. These data agree with reports in hydroxide reactions comparing boron and aluminum reactions using the same SDA¹⁸. Chemical analysis for both hydroxide products shows some sodium incorporation. The measured values correspond to ~0.25 and 0.11 Na/Al for Si/Al=50 and Si/Al=25, respectively. This indicates framework charge was predominantly compensated by SDA rather than alkali. This suggests organic occupies most of the void space within

SSZ-70 in contrast to SSZ-25 where the bulky adamantyl SDA was not expected to fit in the sinusoidal 10MR²⁶.

Table 2.12: Chemical analysis of B-SSZ-70(F), Al-SSZ-70(F) and Al-SSZ-70(OH) products synthesized using **5**

	Gel composition						
	Si/B=18	Si/B=5.5	Si/Al=35	Si/Al=25	Si/Al=15	Si/Al=50	Si/Al=25
C/wt%	13.67	13.51	12.23	13.07	13.54	13.62	13.37
N/wt%	2.80	2.77	2.57	2.71	2.70	2.82	2.81
F/wt%	1.16	1.04	0.70	0.64	0.82	-	-
F/N	0.41	0.38	0.27	0.24	0.30	-	-
Na/wt%	-	-	-	-	-	0.17	0.14
Si/B	21.7	13.7	-	-	-	-	-
Si/Al	-	-	34.1	25.5	16.6	44.4	22.2

In addition to chemical analysis, TGA was performed on SSZ-70 products. Figure 2.12 compares the TG profiles for Si-SSZ-70(F) synthesized using **5** and **8**. Both materials show very similar mass loss between 200 and 620°C (19.3% for **5** and 20.4% for **8**) yet the mass loss profiles were distinct. Smaller bis(isobutyl) **5** shows one mass loss starting at approximately 250°C whereas two mass losses can be seen for the larger bis(cyclohexyl) **8**. The first mass loss starts around 250°C as per **5** with an inflection point at ~425°C followed by another mass loss. Observing two mass loss regions with the larger SDA indicates two distinct organic environments. With SSZ-70 being a layered material the first mass loss was assigned to organic occluded between layers and the second mass loss attributed to organic occluded within the layers. Observing one mass loss with the smaller SDA was likely due to weaker fit within the framework offering lower thermal protection.

Several post-synthesis experiments were performed on an Al-SSZ-70 sample synthesized using **8** to gain insight into the relative contribution of each organic environment. The sample was obtained from the SAR=35 NaY reaction and treated with 1N HCl to neutralize residual FAU species as described in the experimental section. The first experiment explored SDA removal by DMF extraction. Similar experiments with SSZ-25 showed organic removal and significant changes in the XRD pattern after DMF extraction²⁶. No organic removal was detected by TGA after extraction for the Al-SSZ-70 material studied. In addition, the XRD pattern was identical to the parent material. This suggested an organic/framework environment similar to traditional zeolites where extraction does not typically remove organic.

The second experiment thermally treated the as-made material to remove the low-temperature organic material. Inspecting the TGA profiles indicated 350°C was sufficient to remove the first organic environment and should be ~75°C below the mass loss onset of the second environment. After heating at 350°C for five hours in air all organic below 425°C was removed and the XRD pattern showed clear differences. TGA profiles and XRD patterns are shown in Figures 2.13 and 2.14, respectively. The XRD pattern resembled calcined Al-SSZ-70(OH) even though ~7 wt% organic remained occluded. This heat treated material was ammonium-exchanged and assessed for micropore volume and catalytic activity as described below.

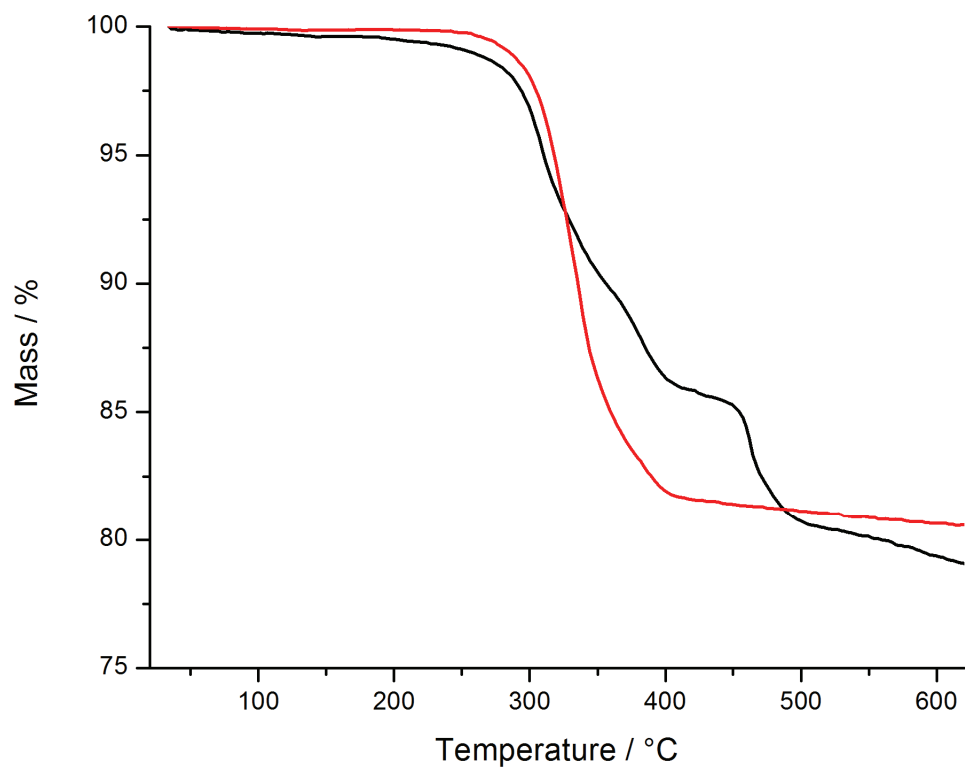


Figure 2.12: TGA of Si-SSZ-70(F) synthesized using **5** (red) and **8** (black)

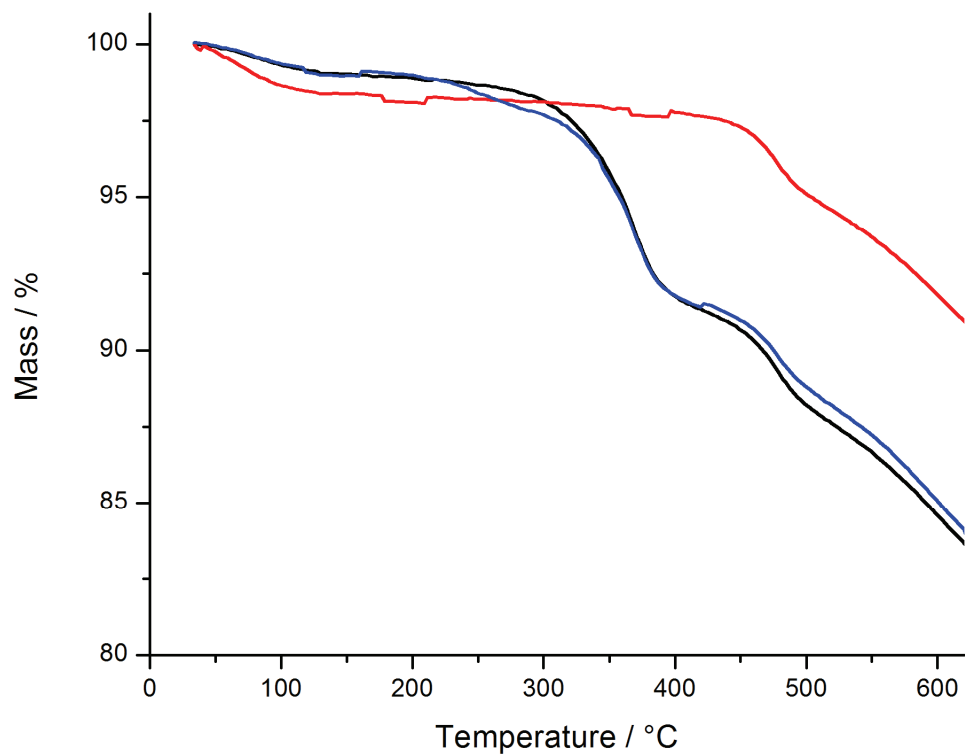


Figure 2.13: TGA of post-synthesis treatments for Al-SSZ-70(OH) synthesized using **8**.

Black=parent material, blue=DMF extracted and red=350°C treated

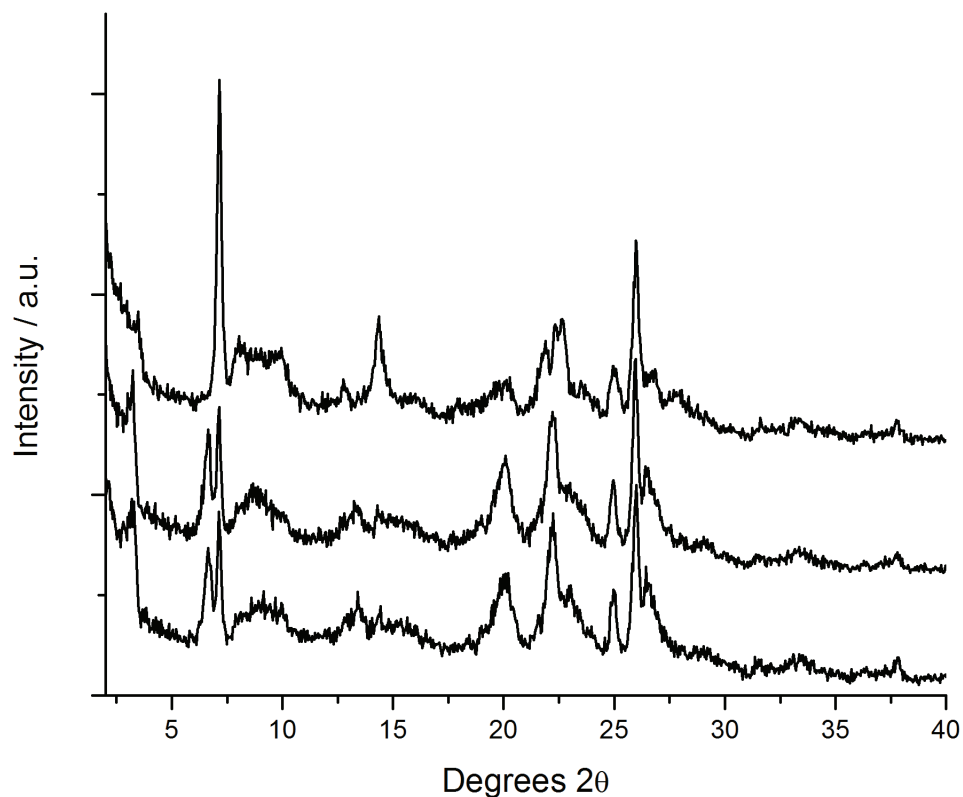


Figure 2.14: XRD patterns of post-synthesis treatments for Al-SSZ-70(OH) synthesized using **8**. Bottom to top: parent material, DMF extracted and 350°C treated

Finally, textural properties of SSZ-70 products were examined using nitrogen adsorption. All SSZ-70 samples examined were synthesized using **5** except Si-SSZ-70(OH) that used **9** and the Al-SSZ-70(OH) 350°C treated sample synthesized using **8**. Table 2.13 lists micropore volume and external surface areas for each SSZ-70 material. These data show a clear distinction between the fluoride and hydroxide products with 0.20 cm³ g⁻¹ micropore volume observed for all three fluoride products and 0.09–0.14 cm³ g⁻¹ observed for the hydroxide products. The micropore volumes for the fluoride products are similar to those reported for MWW materials (0.17–0.18 cm³ g⁻¹). External surface areas typical of zeolites were observed for all products except the two Al-SSZ-70(OH) products.

These materials returned ~ 190 and $100 \text{ m}^2 \text{ g}^{-1}$ external surface area possibly indicating some delamination occurred during heat treatment. The observed external surface areas were significantly lower than those reported for delaminated and exfoliated ITQ-2 ($\sim 700 \text{ m}^2 \text{ g}^{-1}$ external surface area)¹⁴. The 350°C treated material shows $\sim 2/3$ the micropore volume of the calcined Al-SSZ-70(OH) material. Assuming this organic resides in interlayer regions this gives a similar contribution as reported for SSZ-25 where $\sim 0.12 \text{ cm}^3 \text{ g}^{-1}$ micropore volume was attributed to the large cages formed between layers.

Table 2.13: Textural properties of SSZ-70 products

SSZ-70 Product	Micropore volume / $\text{cm}^3 \text{ g}^{-1}$	External surface area / $\text{m}^2 \text{ g}^{-1}$
Si-SSZ-70 (F)	0.20	9
B-SSZ-70 (F)	0.20	37
Al-SSZ-70 (F)	0.20	46
Si-SSZ-70 (OH)	0.09	56
B-SSZ-70 (OH)	0.12	45
Al-SSZ-70 (OH)	0.14	189
Al-SSZ-70 (OH) 350°C treated	0.09	96

2.3.3: Catalytic Activity

Catalytic activity used the constraint index (CI) test as a model acid-catalyzed hydrocarbon reaction. In this reaction the relative cracking rates of n-hexane and 3-methylpentane are used to calculate the constraint index given by the following equation:

$$CI = \frac{\log(\text{n-hexane conv.})}{\log(\text{3-methylpentane conv.})}$$

Four Al-SSZ-70 materials were tested: Al-SSZ-70(F, Si/Al=26) and Al-SSZ-70(OH, Si/Al=22) synthesized using **5** plus Al-SSZ-70(OH) and the 350°C treated material synthesized using **8**. The characterization outlined above showed similarity to MWW materials so SSZ-25 was included for comparison (the SSZ-25 cracking reaction was performed at 330°C). Figure 2.15 shows cracking rate as a function of time on stream (TOS). The three SSZ-70 materials show slight differences in initial cracking rate then converge with increasing TOS. The deactivation with TOS follows a similar path to SSZ-25. The 350°C treated material shows the same deactivation trend although the initial rate was significantly lower than for all other materials owing to lower number of active sites. These data again suggest strong similarity to MWW materials; however, the CI versus TOS shown in Figure 2.16 presents clear distinction. All materials show initial CI values < 1 with SSZ-25 giving a rapid increase as previously described⁴⁰. In contrast, all SSZ-70 materials show CI values < 1.2 throughout. In noting the anomalous SSZ-25 behavior with TOS it was postulated the deactivation rates of the two independent pore systems were different giving rise to changing CI. Both pore systems contribute to initial reactivity, with the more accessible MWW cage dominating over the sinusoidal pore system. The high

initial activity from active sites located within the cages masks the sinusoidal pore reactivity. As active sites in the cages deactivated due to fouling, the sinusoidal pores accounted for relatively higher reactivity resulting in a CI increase to the range expected for medium pore materials ($1 < CI < 12$). All SSZ-70 materials show similar cracking rate deactivation suggesting the presence of a similar cavity, but the absence of increasing CI as the material deactivates suggests a second pore system distinct to the sinusoidal 10MR pore found in MWW. Additional catalytic tests and adsorption studies^{41, 42} might offer insight into the structure of SSZ-70; however, a structural model should be the ultimate aim.

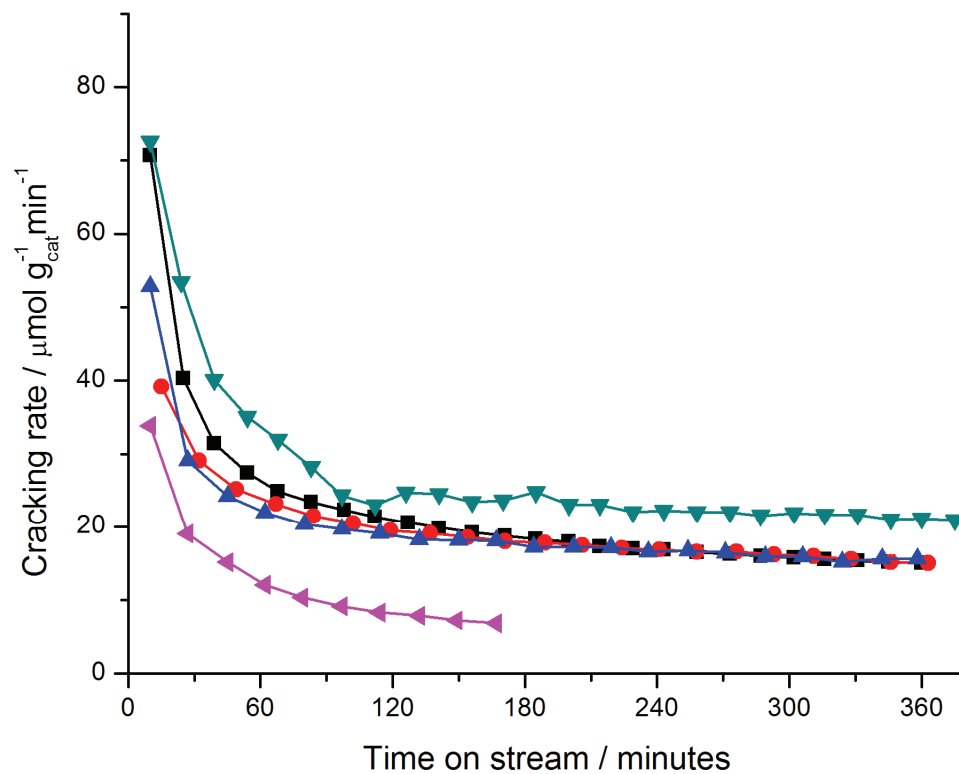


Figure 2.15: CI test cracking rate vs. time on stream for Al-SSZ-70 materials. SSZ-25(▼), Al-SSZ-70(F)(●), Al-SSZ-70(OH-5)(▲), Al-SSZ-70(OH-8)(■) and Al-SSZ-70(OH-8 350°C treated)(◄)

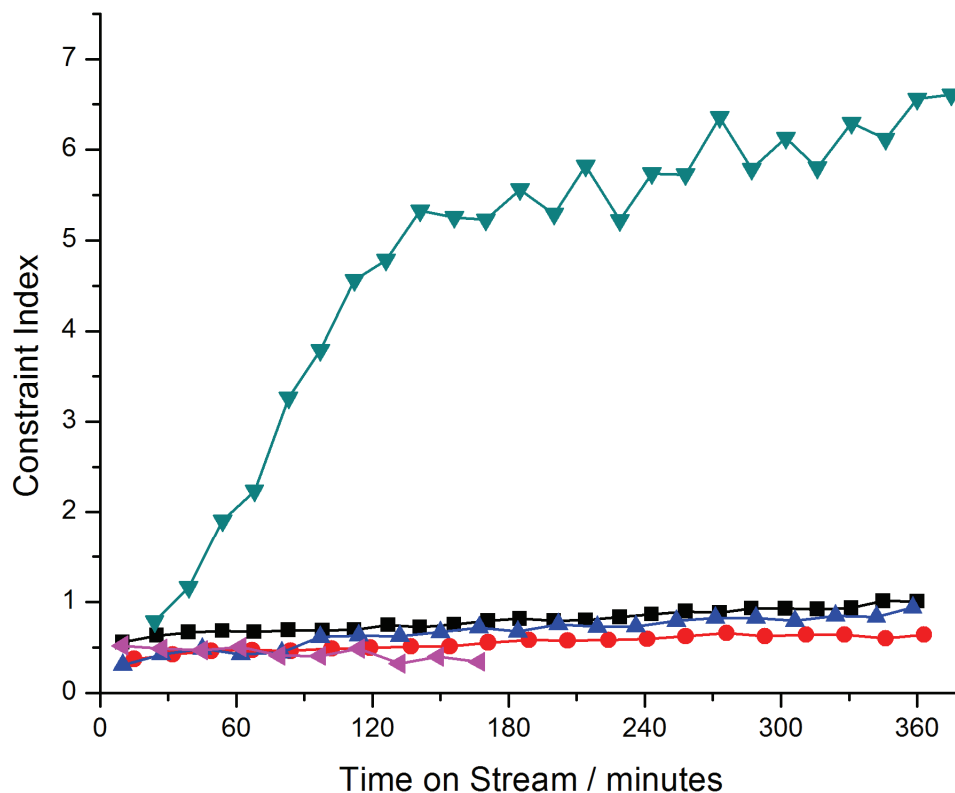


Figure 2.16: Constraint index vs. time on stream for Al-SSZ-70 materials. SSZ-25(▼), Al-SSZ-70(F)(●), Al-SSZ-70(OH-5)(▲), Al-SSZ-70(OH-8)(■) and Al-SSZ-70(OH-8 350°C treated)(◄)

2.4: Conclusions

Investigating guest/host relationships for a library of 16 imidazolium SDAs found eight guest molecules synthesized SSZ-70. The original synthesis under boron-rich conditions using **3** was expanded to pure-silica and aluminosilicate SSZ-70 under both fluoride and hydroxide conditions. Characterization by XRD, ^{29}Si MAS NMR, electron microscopy and nitrogen adsorption showed similarity to MWW materials. Catalytic tests on Al-SSZ-70 revealed active catalytic behavior with distinct differences to SSZ-25.

2.5: Acknowledgments

This work was performed in collaboration with S.I. Zones, A.W. Burton (both from Chevron Energy Technology Company), J.R. Carpenter and S.J. Hwang (both from California Institute of Technology). Several inorganic reactions with **1–3** were performed by SIZ and XRD analysis by AWB. Catalytic tests were performed by JRC and ^{29}Si NMR spectra were recorded by SJH. In addition, electron microscopy was performed by I.Y. Chan (Chevron Energy Technology Company).

2.6: References

1. S. I. Zones and A. W. Burton, US Patent No. 7,108,843 (2006).
2. S. I. Zones, R. J. Darton, R. Morris and S. J. Hwang, *Journal of Physical Chemistry B* **109** (1), 652–661 (2005).
3. S. I. Zones, *Zeolites* **9** (6), 458–467 (1989).
4. A. W. Burton, *Journal of the American Chemical Society* **129** (24), 7627–7637 (2007).
5. S. I. Zones, S. J. Hwang, S. Elomari, I. Ogino, M. E. Davis and A. W. Burton, *Comptes Rendus Chimie* **8** (3–4), 267–282 (2005).
6. S. I. Zones, US Patent No. 4,483,835 (1984).
7. J. March and M. B. Smith, *March's Advanced Organic Chemistry: Reactions, Mechanisms, and Structure*, 5th ed. (Wiley-Interscience, 2001).

8. A. J. Arduengo, R. L. Harlow and M. Kline, *Journal of the American Chemical Society* **113** (1), 361–363 (1991).
9. A. J. Arduengo, *Accounts of Chemical Research* **32** (11), 913–921 (1999).
10. M. E. Leonowicz, J. A. Lawton, S. L. Lawton and M. K. Rubin, *Science* **264** (5167), 1910–1913 (1994).
11. A. Corma, M. J. Díaz-Cabanas, M. Moliner and C. Martínez, *Journal of Catalysis* **241** (2), 312–318 (2006).
12. G. G. Juttu and R. F. Lobo, *Microporous and Mesoporous Materials* **40** (1–3), 9–23 (2000).
13. W. J. Roth, C. T. Kresge, J. C. Vartuli, M. E. Leonowicz, A. S. Fung and S. B. McCullen, *Catalysis by Microporous Materials* **94**, 301–308 (1995).
14. A. Corma, V. Fornes, S. B. Pergher, T. L. M. Maesen and J. G. Buglass, *Nature* **396** (6709), 353–356 (1998).
15. C. Y. Chen, S. I. Zones, S. J. Hwang, A. W. Burton and A. J. Liang, in *Studies in Surface Science and Catalysis (From Zeolites to Porous MOF Materials— the 40th Anniversary of International Zeolite Conference)*, edited by R. R. Xu, Z. Gao, J. Chen and W. Yan (Elsevier 2007), Vol. 170.
16. T. Ikeda, Y. Akiyama, Y. Oumi, A. Kawai and F. Mizukami, *Angewandte Chemie-International Edition* **43** (37), 4892–4896 (2004).
17. C. Y. Chen and S. I. Zones, in *Studies in Surface Science and Catalysis (Zeolites and Mesoporous Materials at the Dawn of the 21st Century: Proceedings of the 13th International Zeolite Conference)*, edited by A. Galarneau, F. Di Renzo, F. Fajula and J. Viedrine (Elsevier, 2001), Vol. 135.

18. S. I. Zones and S.-J. Hwang, *Microporous and Mesoporous Materials* **58** (3), 263–277 (2003).
19. S. I. Zones, M. M. Olmstead and D. S. Santilli, *Journal of the American Chemical Society* **114** (11), 4195–4201 (1992).
20. W. A. Herrmann, V. P. W. Bohm, C. W. K. Gstottmayr, M. Grosche, C. P. Reisinger and T. Weskamp, *Journal of Organometallic Chemistry* **617** (1), 616–628 (2001).
21. W. A. Herrmann, C. Kocher and L. J. Goossen, US Patent No. 6,025,496 (2000).
22. A. K. Burrell, R. E. Del Sesto, S. N. Baker, T. M. McCleskey and G. A. Baker, *Green chemistry* **9** (5), 449–454 (2007).
23. A. Jackowski, S. I. Zones, S.-J. Hwang and A. W. Burton, *Journal of the American Chemical Society* **131** (3), 1092–1100 (2009).
24. V. J. Frillette, W. O. Haag and R. M. Lago, *Journal of Catalysis* **67** (1), 218–222 (1981).
25. S. I. Zones, Y. Nakagawa, G. S. Lee, C. Y. Chen and L. T. Yuen, *Microporous and Mesoporous Materials* **21** (4–6), 199–211 (1998).
26. S. I. Zones, S. J. Hwang and M. E. Davis, *Chemistry—a European Journal* **7** (9), 1990–2001 (2001).
27. X. B. Yang, M. A. Camblor, Y. Lee, H. M. Liu and D. H. Olson, *Journal of the American Chemical Society* **126** (33), 10403–10409 (2004).
28. M. A. Camblor, P. A. Barrett, M.-J. Díaz-Cabañas, L. A. Villaescusa, M. Puche, T. Boix, E. Pérez and H. Koller, *Microporous and Mesoporous Materials* **48** (1–3), 11–22 (2001).

29. Y. Chu, H. Deng and J. P. Cheng, *Journal of Organic Chemistry* **72** (20), 7790–7793 (2007).
30. T. Fahlbusch, M. Frank, J. Schatz and D. T. Schuhle, *Journal of Organic Chemistry* **71** (4), 1688–1691 (2006).
31. P. Wagner, M. Yoshikawa, M. Lovallo, K. Tsuji, M. Taspatsis and M. E. Davis, *Chemical Communications* (22), 2179–2180 (1997).
32. R. F. Lobo, S. I. Zones and R. C. Medrud, *Chem. Mater.* **8** (10), 2409–2411 (1996).
33. N. M. Scott and S. P. Nolan, *European Journal of Inorganic Chemistry* (10), 1815–1828 (2005).
34. M. A. Cambor, A. Corma, M. J. Diaz-Cabanas and C. Baerlocher, *J. Phys. Chem. B* **102** (1), 44–51 (1998).
35. M. A. Cambor, C. Corell, A. Corma, M.-J. Diaz-Cabanas, S. Nicolopoulos, J. M. Gonzalez-Calbet and M. Vallet-Regi, *Chemistry of Materials* **8** (10), 2415–2417 (1996).
36. H. Koller, A. Wolker, L. A. Villaescusa, M. J. Diaz-Cabanas, S. Valencia and M. A. Cambor, *Journal of the American Chemical Society* **121** (14), 3368–3376 (1999).
37. I. Y. Chan, P. A. Labun, M. Pan and S. I. Zones, *Microporous Materials* **3** (4–5), 409–418 (1995).
38. H. Koller, R. F. Lobo, S. L. Burkett and M. E. Davis, *Journal of Physical Chemistry* **99** (33), 12588–12596 (1995).
39. R. Aiello, F. Crea, F. Testa, G. Demortier, P. Lentz, M. Wiame and J. B. Nagy, *Microporous and Mesoporous Materials* **35–36**, 585–595 (2000).

40. S. I. Zones and T. V. Harris, *Microporous and Mesoporous Materials* **35–36**, 31–46 (2000).
41. C. Y. Chen and S. I. Zones, *Microporous and Mesoporous Materials* **104** (1–3), 39–45 (2007).
42. S. I. Zones, C. Y. Chen, A. Corma, M. T. Cheng, C. L. Kibby, I. Y. Chan and A. W. Burton, *Journal of Catalysis* **250** (1), 41–54 (2007).